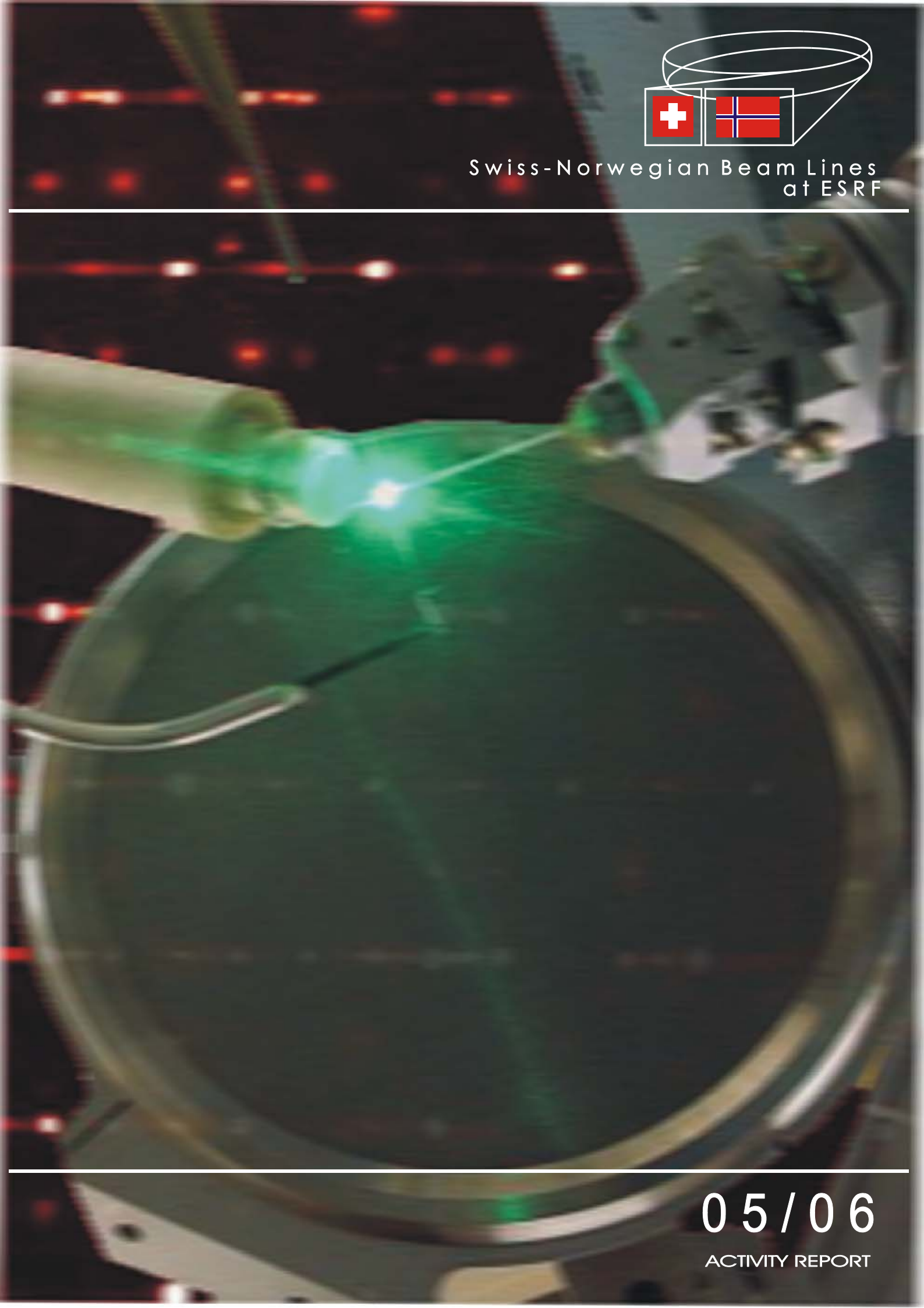

Swiss-Norwegian Beam Lines
at ESRF

05/06

ACTIVITY REPORT

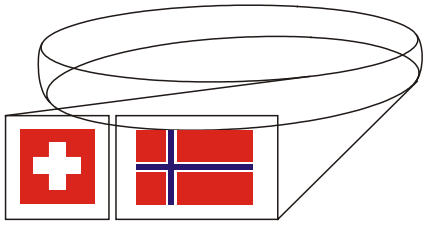

Swiss-Norwegian Beam Lines
at ESRF

Contents ***Page***

The years 2005-2006 served both to conclude the important, initial ten-years in the operational life of SNBL, and to define the direction of its further development. At the end of the first decade of the SNBL operations, the question was raised concerning the optimal configuration of the beam lines. Should the variety of techniques existing at the two end-stations be reduced in order to make the beam lines more specialised? In other words, should SNBL follow an example of beam lines at large-scale facilities and become a high performance scientific tool only suitable for solving very specific problems? All financial and human resources, in the case, should be invested into a specialised "state-of-the art" beam line. The new SNBL management, however, has seen a different future for the beam lines. This view was formed after discussions with our user community; it had strong links to their research strategy, and aimed to providing the most appropriate assistance to their projects, both those already running and others still in planning. The beam lines were seen as multifunctional, dedicated to complex *in situ* experiments requiring combinations of diffraction and spectroscopic techniques. This approach received full support from both the SNX Council and national science foundations.

The present report highlights a few examples of work done at SNBL of the "second generation". We briefly review of our solid financial and material base, and we summarize the content and quality of the papers published during last two years by research groups who have worked at SNBL. Even at a quick glance, the decision taken two years ago seems to be bearing fruit. The efficiency and productivity of the beam lines has increased – at present about 75% of projects finalize with publication. The quality of publications is increasing too – the average impact factor has steadily risen, and now approaches the level of a Physical Review journal.

Two key factors account for the success of the facility. First of all, there is the pro-active role of our users in forming the strategy and tactics of the SNBL development. We are pleased to acknowledge their intellectual and material contributions into our common progress. The second definitive factor is enormous enthusiasm of the SNBL staff in making technical improvements, analysing the trends in the evolution of the user community, suggesting solutions to ensure further progress, and, last but not least, providing a high-quality service on the beam lines. One can conclude that SNBL became, in some aspects, a "national laboratory" for many user groups. The best indication of this role is the increasing number of students sent to SNBL by the research laboratories, who come to Grenoble in order to pass a period of training or to participate in development of an individual experimental setup. It allows us to believe in a successful and prosperous future for our shared project named SNBL.

V. DMITRIEV, P. PATTISON, H. EMERICH

SCIENTIFIC HIGHLIGHTS

Tyrolite: from 1817 to 2006

Sergey V. Krivovichev[1,2], Dmitry Yu. Chernyshov[3], Nicola Döbelin[4], Thomas Armbruster[4], Volker Kahlenberg[2], Reinhard Kaindl[2], Giovanni Ferraris[5], Richard Tessadri[2], and Gerard Kaltenhauser[2]

[1] Department of Crystallography, Faculty of Geology, St.Petersburg State University, St.Petersburg (Russia)
[2] Institut für Mineralogie und Petrographie, Universität Innsbruck (Austria)
[3] SNBL at the ESRF (France)
[4] Laboratorium für chemische und mineralogische Kristallographie, Universität Bern, Freiestrasse 3, CH-3102 Bern, Switzerland
[5] Dipartimento di Scienze Mineralogiche e Petrologiche Università di Torino (Italy)

Copper arsenates are common minerals in oxidation zones of sulfide ore deposits. There are more than 70 different copper arsenate mineral species reported so far. The restricted stability of arsenic-bearing minerals such as the copper arsenates may play a significant role in the mobility of arsenic in the near-surface environment. Structural investigations of secondary As-bearing phases may lead to a better understanding of the geochemical behavior of As and thereby help to elucidate mechanisms of transportation and accumulation of As under natural conditions.

Tyrolite, a complex copper arsenate carbonate hydrate, was first described by A.G. Werner in 1817 from Schwaz-Brixlegg, Tyrol, Austria. The mineral is widely distributed and has been reported to be found at more than 128 localities worldwide. Crystal structure of tyrolite was unknown, primarily due to the poor quality of their platy and flexible crystals. Recently, we have reported the crystal structures of two tyrolite polytypes, which were solved using the experimental advantages provided by modern area detector technologies and high-intensity synchrotron radiation.

The samples of tyrolite used in this study originate from the tyrolite type locality (Brixlegg, Schwaz, Tyrol). One of the samples represented a dolomite rock covered by greenish-blue flexible tyrolite crystals (Fig. 1). All attempts to collect indexable X-ray diffraction data from relatively large crystals extracted from this sample were unsuccessful. In all cases, only two unit-cell parameters could be reliably determined, whereas the third could not be found. Close inspection of the sample revealed two visually different aggregates: light blue plates and aggregates of greenish-blue elongated platy crystals. One of the greenish-blue aggregates was split and several strongly birefringent plates were selected under a polarization microscope. X-ray diffraction experiments were performed under ambient conditions at the Swiss – Norwegian beamline BM01A of the

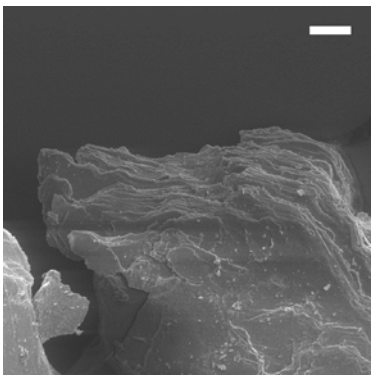

Fig. 1. Crystals of tyrolite from Brixlegg-Schwaz, Tyrol. Scale bar is 50 µm.

European Synchrotron Research Facility (ESRF) using an imaging plate area detector (Mar345) with a crystal-to- detector distance of 150 mm. Data were collected for the crystal with dimensions of 11 × 14 × 2 μm^3. Diffraction data were measured using monochromatic radiation (λ = 0.80000 Å) in an oscillation mode by rotating the crystal in φ by 2° in 2 min per frame; 179 frames were measured. The structure was solved using SHELXS program. The agreement factor for the final model is R_1 = 0.089 for 2522 unique observed reflections with $|F_o| \geq 4\sigma_F$.

Structure description

Fig. 2 shows projection of the structure of tyrolite-1*M* along the *b* axis. It is based upon complex slabs consisting of Cu, As, and Ca coordination polyhedra. The slabs are about 26 Å = 2.6 nm thick and thus can be considered as nanolayers. This feature of the structure of tyrolite is very specific and has not been previously observed in oxysalt minerals. The architecture of the nanolayers can be understood in terms of separate sublayers. The core of the nanolayer is a copper arsenate substructure consisting of the **A** and **B** sublayers specified in Fig. 3. The **B** sublayer represents a series of chains of edge-sharing Cu octahedra running along the *b* axis. Within the chain, three $Cu^{2+}\varphi_6$ octahedra form trimers by sharing the common OH group. Similar trimeric units constitute an important part of the **A** sublayer. However, in this case, the trimers do not form chains but share corners with AsO_4 tetrahedra to produce a complex 2-dimensional topology. The copper arsenate substructure consists of two **A** sublayers linked by the octahedral chains from the **B** sublayer resulting in formation of the 18Å-thick **ABA** slab. The **ABA** copper arsenate slab is sandwiched between the sublayers of the Ca^{2+} cations and H_2O molecules. The adjacent nanolayers are connected by hydrogen bonds to the interlayer species.

.

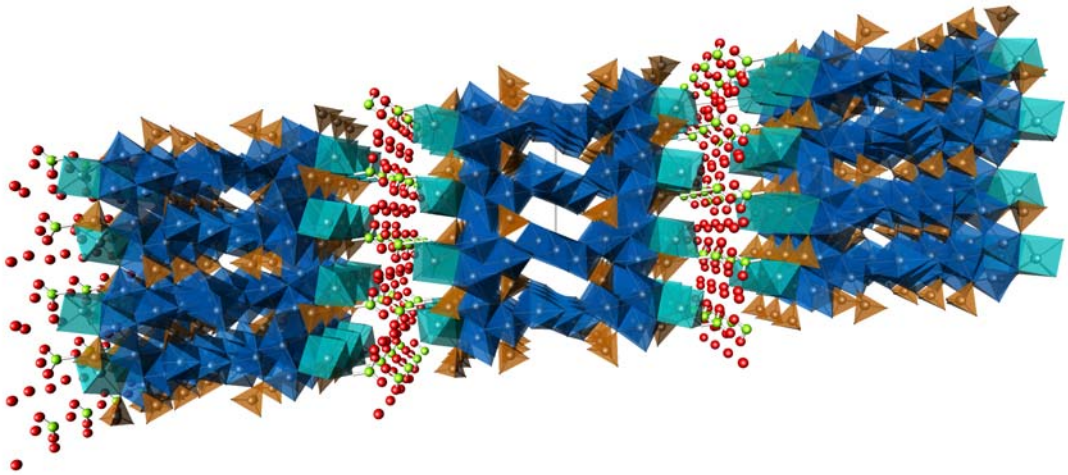

Fig. 2. Crystal structure of tyrolite viewed parallel to the *b* axis (perspective view). Cu, As, and Ca polyhedra are blue, brown, and light-blue, respectively; O and H_2O groups are red, C atoms of the carbonate groups are light-green.

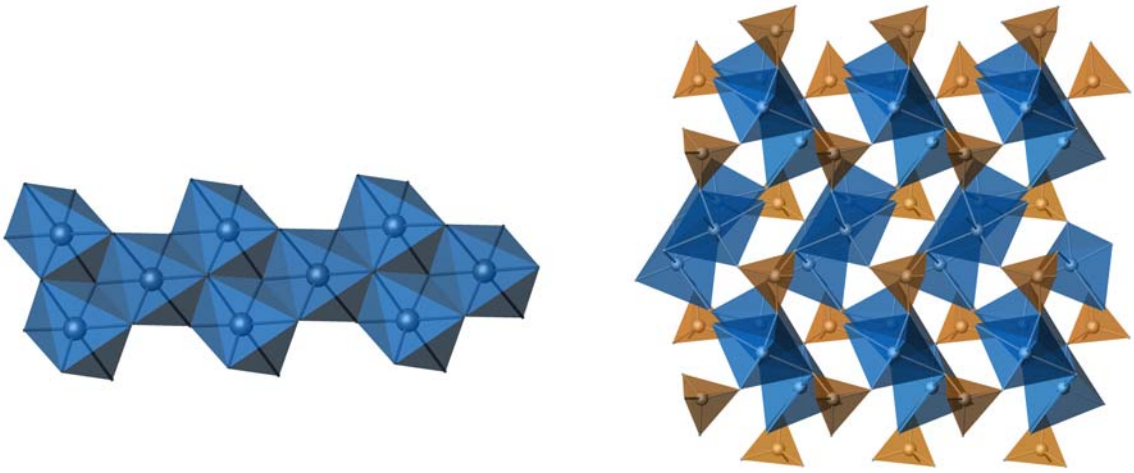

Fig. 3. Chains of trimeric units of Jahn-Teller distorted Cu octahedra (left) constituting the B sublayer and layer of Cu octahedral trimers interlinked through AsO_4 tetrahedra (A sublayer) (right).

The structure of tyrolite-2*M* is very similar to that of tyrolite-1*M* and differs from the latter by the stacking sequence of the nanolayers. In both structures, adjacent nanolayers are translationally equivalent. The adjacent nanolayers in tyrolite-2*M* are shifted by *b*/2 = 2.8 Å in comparison to the relative position of the nanolayers in tyrolite-1*M*. This shift is quite subtle compared to the thickness of the nanolayers (26 Å). Perhaps, this feature of the tyrolite polytypes explains the difficulties associated with the structural characterization of this mineral.

The unique character of the structures of tyrolite polytypes described here (nanometer-sized layers linked by weak hydrogen bonds) makes it interesting from the viewpoint of material science. Recently, much attention as been attracted by the layered materials with weak interlayer bonding. Using specific experimental procedures, these materials can be exfoliated into nanosheets with subsequent fabrication of nanomaterials (e.g. by rolling nanosheets into nanotubes or by intercalating of organic molecules in between the layers and fabrication of organic/inorganic nanocomposites). Tyrolite polytypes are especially interesting in this regard owing to the magnetism of the Cu^{2+} cations. In tyrolites, 2-dimensional nanosized substructure of transition metal ions (Cu^{2+}) is sandwiched between the layers of dielectric Ca^{2+} cations and H_2O molecules. This peculiarity of the tyrolite structure makes it very interesting from the viewpoint of physical properties, which are currently under investigation.

Publication: Krivovichev, S.V., Chernyshov, D.Y., Döbelin, N., Armbruster, Th., Kahlenberg, V., Kaindl, R., Ferraris, G., Tessadri, R., Kaltenhauser, G. *Crystal chemistry and polytypism of tyrolite* American Mineralogist, 91, 1378-1384, 2006

Novel adsorption behavior of Carbon Dioxide in the isotypic nanoporous metal terephthalate MIL-53

Philip L. Llewellyn, Sandrine Bourrelly, Christian Serre, Thomas Devic and Gérard Férey
(Marseille and Versailles)

One of the technological problems that face society today is the environmentally friendly and economically favourable separation and recovery of gases. Examples of current interest include the recovery of greenhouse gases (CO_2, CH_4) and the purification of hydrogen produced from biomass. Parts of these processes include an adsorption step in which microporous adsorbents such as activated carbon and zeolites are used. In such cases, it is the thermal regeneration step that is most costly in terms of energy.

Recent interest has focused on “Metal Organic Frameworks” (MOF) which are formed of metallic centres linked to each other through organic chains. Several of these organic-inorganic hybrid porous solids have the interesting feature, during adsorption, of being selectively flexible (breathing) as a function of the nature of the adsorptive fluid. A consequence of this particular property is the possibility to develop novel selective separation and storage processes with a favourable energetic cost with respect to already existing processes.

The structural topology of MIL-53(Cr) [1-3] corresponds to a 4^4 net (Fig.1). It consists of tilted chains of $Cr^{III}O_4(OH)_2$ octahedra sharing trans hydroxyl groups. These chains are linked via carboxylate groups of the terephthalate ions (1,4-benzene dicarboxylate or BTC) forming a 3-D framework.

The resulting pore system is one-dimensional of free diameter close to 0.85 nm. The chemical formula of the metal-benzenedicarboxylate is $Cr(OH)(O_2C–C_6H_4–CO_2)$. The sample was synthesised by the group in Versailles following a previously published protocol [3].

To understand the adsorption process we try to couple adsorption experiments up to 50 bars with in situ measurements such as calorimetry and XRD.

The direct calorimetric measurements obtained during adsorption give information on the energetic nature of adsorbents which can be of importance to characterize solids in terms of specific adsorption sites and defects. Moreover, such information is of great interest for defining the adsorbent performance in process design.

The isotherms (Fig. 2) show the adsorption of CO_2 and CH_4 on MIL53(Cr) at 303K. The upper curves show results on samples outgassed until free of residual water. It can be seen that the behaviour of CH_4 is much like the adsorption on other nanoporous materials such as zeolites. However the adsorption of CO_2 shows a distinct step [5]. The latter proceeds in two stages after a very fast uptake at low pressure (~2-3 $mmol.g^{-1}$), the isotherm reaches first a plateau between 1 and 4 bars, followed by an adsorption of more than a double amount of CO_2 at higher

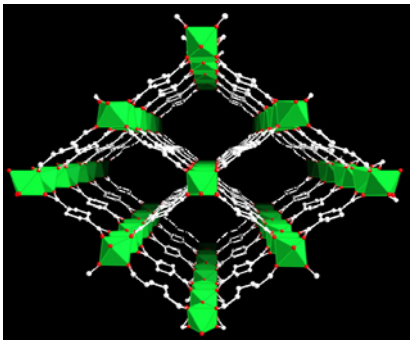

Fig. 1 : Schematic diagram of the pore system of MIL53.

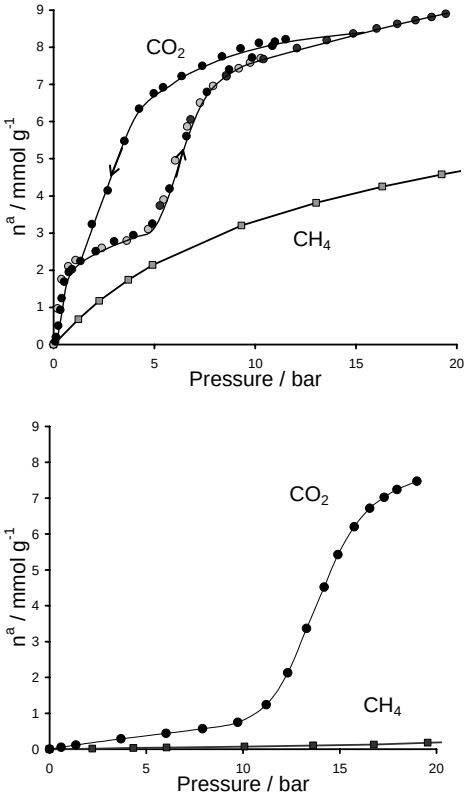

Fig. 2 : CO_2 and CH_4 adsorption isotherms obtained at 303 K on the dehydrated (upper curves) and hydrated (lower curves) forms of MIL53(Cr).

pressures. Interestingly, desorption occurs with a hysteresis loop with the desorption branch returning to the adsorption one at *ca*. 2 bar.

The differential enthalpies of adsorption obtained with the dehydrated sample are shown in Figure 3. It can be seen that the initial adsorption occurs with an enthalpy of around -30 kJ mol^{-1}. The enthalpy then increases sharply. The second adsorption step is accompanied by a large decrease in the enthalpies and at the end of this second step, the enthalpies increase once again.

The differential enthalpies of adsorption obtained with the dehydrated sample are shown in Figure 3. It can be seen that the initial adsorption occurs with an enthalpy of around -30 kJ mol^{-1}. The enthalpy then

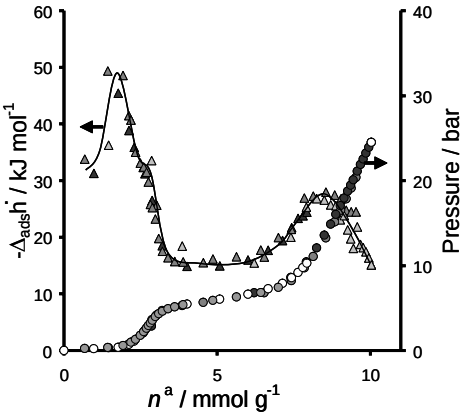

Fig. 3 : Enthalpies and isotherm obtained for CO_2 adsorption at 303 K on dehydrated MIL53(Cr).

increases sharply. The second adsorption step is accompanied by a large decrease in the enthalpies and at the end of this second step, the enthalpies increase once again.

The evolution of the adsorption enthalpies are quite surprising. Such variations could be due to an initial adsorption on localised sites followed by the filling of the remaining porosity. A second hypothesis is that the adsorption phenomena are due to a change in the structure of the porous phase. This hypothesis emanates from the fact that this structure undergoes a contraction on contact with residual water vapour [6].

To follow the structure of the solid phase, experiments were carried out on an adsorption system adapted for *in situ* X-ray diffraction experiments. The results obtained for the dehydrated system are shown in Fig. 4. The diffractograms show that the dehydrated sample is in the open form. The initial dose of carbon dioxide closes the structure. This closed structure remains to a pressure of around 6-7 bars at which point the opening of the structure is observed. This corresponds to the second step in the isotherm. On desorption, the open structure is maintained to a pressure of around 2 bars at which the structure closes once

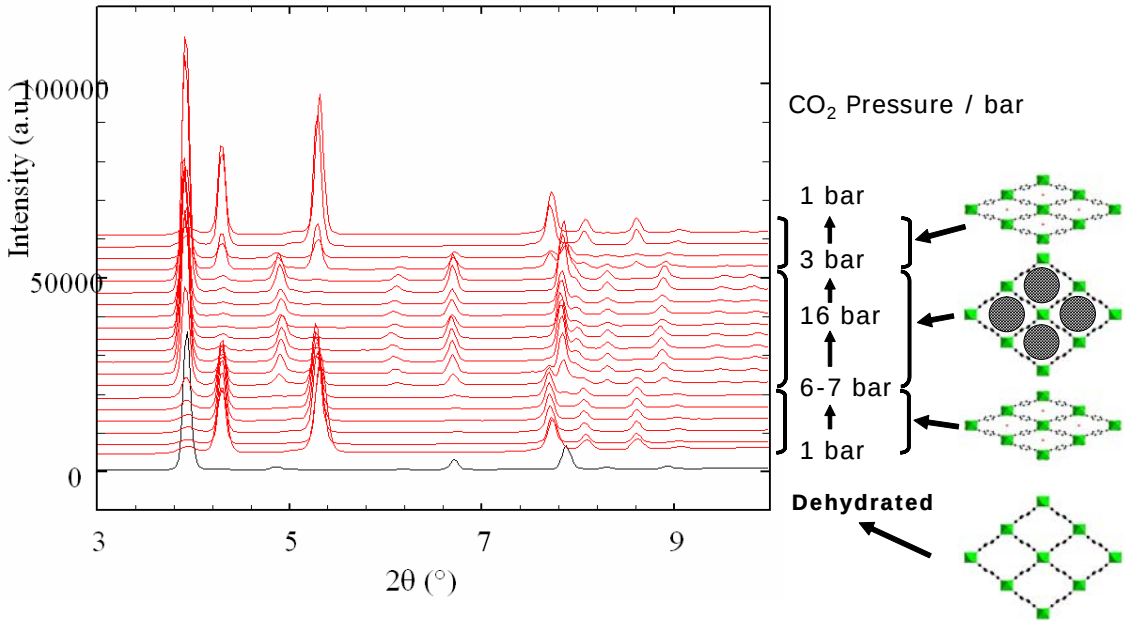

Fig. 4. X-ray diffraction spectra obtained on adsorption and desorption of CO_2 on the dehydrated MIL-53(Cr) sample.

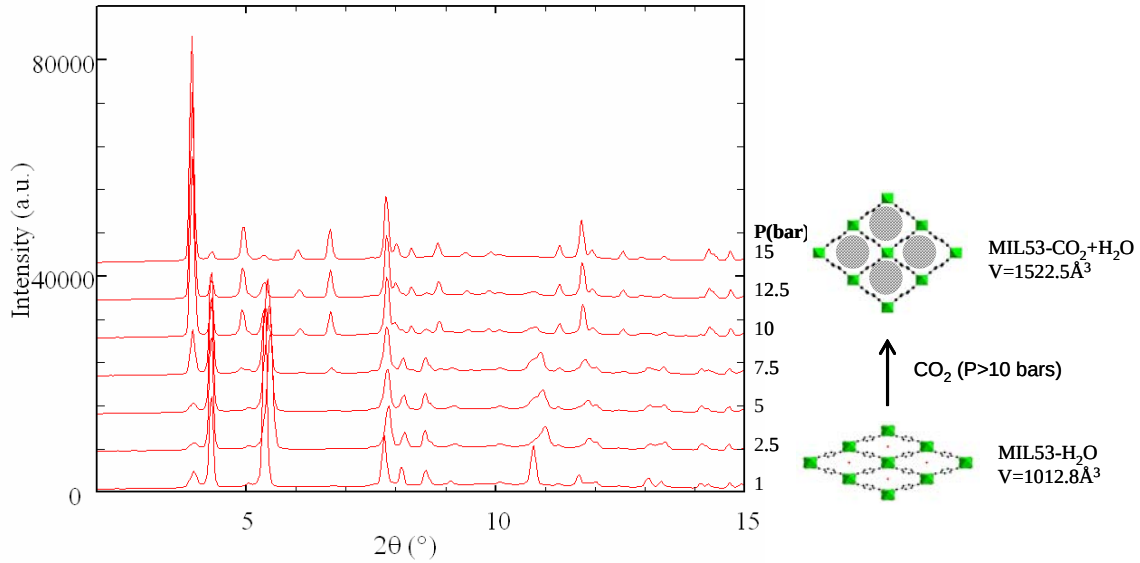

Fig. 5. X-ray diffractogram obtained on adsorption of CO_2 on the hydrated MIL-53 (Cr).

again. Interestingly, the pore contraction, which occurs in MIL-53 upon adsorption of CO_2 at 1 bar is slightly lower than that in the case of hydration: the unit cell shrinks to 1072 $Å^3$ in the case of the closed MIL53 (Cr) structure with CO_2 compared to ~1012 $Å^3$ for the hydrated structure. This would be consistent with the larger size of CO_2 compared to H_2O. The isotherms shown in Fig. 2 (lower curves) show the adsorption of CO_2 and CH_4 on MIL53(Cr) which has been left in

the presence of humidity [7]. It has previously been shown that under such conditions the MIL53 is in a closed form [6] and thus virtually no CH_4 is adsorbed. However, there is an adsorption of CO_2 above 12 bars. The in situ X-ray diffraction (Figure 5) again allows an insight into the adsorption phenomena. As expected, the hydrated form of the MIL53(Cr) is contracted. The opening of the structure occurs in the region from 7.5 to 10 bars. With decreasing pressures (not shown), the desorption branch in the isotherm corresponds to a contraction of the MIL53 structure. Interestingly, the closed structure after desorption has the same cell volume as that observed during the initial adsorption of CO_2 on the dehydrated sample. Note also that the desorption branch on the hydrated sample does no rejoin the adsorprtion branch and that the final point corresponds to around 2 mmol g^{-1} which is a similar value to that observed with the dehydrated sample. These facts point to a replacement of the water in the hydrated sample by carbon dioxide.

Such results are of major significance for future applications in gas separation and storage. It can be appreciated that the important feature of the above results is that the apparent selectivity is drastically increased for the hydrated sample. That is to say that the relative amount of CO_2 adsorbed with respect to CH_4 is increased for the hydrated material. This is not the case for other carbon dioxide adsorbents such as zeolites where often the water blocks specific sites. It has previously been shown that the present sample is stable to higher humidity and thus a process where a significant amount of water is present may not harm the adsorption of carbon dioxide. Thus the need for a preadsorber in a PSA type process would not be required thus leading to simpler process design. Further work on the adsorption of carbon dioxide in the presence of increasing partial pressures of water is planned.

This work highlights the difference in adsorption behaviour between a polar and non-polar probe. To make a generalisation, it will be of importance to follow other molecules of varying polarity. Nevertheless, the above results are particularly interesting when one considers the recovery of carbon dioxide in mixed gas streams or the use of such materials in sensor type applications. As it would initially seem that the structural flexibility of these materials is related to the polar nature of the probe gas molecule, such results could pave the way for the use highly flexible MOFs for the separation of other mixtures of polar and non-polar gases. Initially, it will be of interest to study the feasibility to recover CO_2 in natural gas feeds in which the water content is significant.

This work was supported by EU funding via FP6-Specific Targeted Research Project “DeSANNS” (SES6-020133).

[1] K. Barthelet, J. Marrot, D. Riou, G. Férey, *Angew. Chem. Int. Ed*., 41, (2002), 281-284.
[2] T. Loiseau, C. Mellot-Draznieks, H. Muguerra, G. Férey, M. Haouas, F. Taulelle, *C. R. Chimie,* 8(3-4), (2005), 765-772.
[3] C. Serre, F. Millange, C. Thouvenot, M. Noguës, G. Marsolier, D. Louër, G. Férey, *J. Am. Chem. Soc*., 124, (2002), 13519-13526.
[4] P. L. Llewellyn, G. Maurin, *C. R. Chimie,* 8, (2005), 283.
[5] S. Bourrelly, P. L. Llewellyn, C. Serre, F. Millange, T. Loiseau, G. Férey, *J. Am. Chem. Soc*., 127(39), (2005), 13519-13521.
[6] T. Loiseau, C. Serre, C. Huguenard, G. Fink, F. Taulelle, M. Henry, T. Bataille, G. Férey, *Chem. Eur. J.,* 10, (2004), 1373-1382.
[7] P. L. Llewellyn, S. Bourrelly, C. Serre, Y. Filinchuk, G. Férey, *Angew. Chem. Int. Ed*. 45(46), (2006), 7751-7754

Interplay of spin conversion and structural phase transformations.

Karl W. Törnroos,[a] Marc Hostettler,[b] Dmitry Chernyshov,[c] Brita Vangdal,[a] and Hans-Beat Bürgi[b]

[a] Department of Chemistry, University of Bergen, (Norway)
[b] Laboratorium für Kristallographie, Universität Bern (Switzerland)
[c] SNBL at the ESRF, (France)

Much of the continuing activity in spin crossover research on octahedral complexes with 3d metals is motivated by potential applications for display, memory and switching devices.[1,2,3] In the solid state, molecular bi-stability is only one factor governing the changes of physical properties, another being the interactions between the ions and molecules in a crystal. The complex interplay between molecular and crystal properties produces solid-state phenomena including not only bi-stability, but also multi-stability as well as complete suppression of changes in physical properties.

We have recently reported on magnetic and calorimetric measurements as well as on a multi-temperature single-crystal diffraction study of the $[Fe^{II}(2\text{-pic})_3]Cl_2 \cdot 2$-propanol solvate (**1**).[4] The crystal structure has been measured at 21 temperatures, 14 of them covering a cooling cycle from 293 to 15 K, and 7 a heating cycle between 149 and 206 K. The transition curve based on magnetic data is thus endorsed by a microscopic characterization of the thermal evolution of the crystal structure.

The 2-propanol solvate, **1**, and the ethanol analogue [5] are chemically and structurally very similar and they both show two consecutive, re-entrant structural phase transitions and solvent ordering on cooling. There are important qualitative and quantitative differences, however. In the ethanol solvate, ordering occurs at a ~50% high spin (HS) concentration, whereas for **1** it happens near ~95%. In the former, the high spin (HS) and low spin (LS) species within a hydrogen-bonded layer order – nearly completely - in a chessboard-like pattern, whereas in **1** they form an arrangement of alternating zigzag chains; the complexes in one chain are nearly all HS and those in the other present a disordered mixture of HS and LS states (Figure 1). The two compounds also differ in the temperature evolution of the solvent disorder. All these differences are achieved by simply changing an ethyl group for a 2-propyl group in an otherwise unchanged crystal architecture. There must thus be factors influencing the transition scenario other than the ligand field; vibrational contributions and different degrees of disorder of the solvent molecules are but two of them.

Hysteresis behaviour marks another difference between the two solvates: no hysteresis has been found for the ethanol derivative, while a distinct triangular hysteresis loop is observed for **1** at the low-temperature side of the HS intermediate phase (IP) (Figure 2). Within this loop macroscopic domains of the HS IP and of the disordered LS/HS zone of the low-temperature phase coexist, a conclusion that follows from the simultaneous appearance of Bragg reflections from both phases at ~153 K.

For both the ethanol and 2-propanol solvates, the ordering processes of the solvate molecules and its coupling to spin conversion have been expressed with a Landau expansion amended with an Ising-like free energy for the genuine spin conversion process [4]. The resulting model is capable of mapping a

plateau in the transition curve centered at any critical HS concentration. By virtue of the coupling terms, it also accounts for the different spin crossover behavior of the two different sites in the HS IP of **1**. The rather drastic changes of the size and the shape of the unit cell with temperature (Figure 3) may be taken into account by bringing in a coupling between lattice strains and order parameters. Thus a simple phenomenological approach uncovers the generic nature of multi-stability in spin crossover solids, namely coupling between single-site spin crossover and collective degrees of freedom accounting for structural ordering.

Changes in solvent disorder not only contribute to changes in entropy during the spin crossover process, but may also trigger the transition. The diffraction study of **1** shows that the OH···Cl and the NH···Cl hydrogen bonds may change by as much as 0.1 Å across the phase transitions. Similarly the orientation of the pyridine rings relative to the *a*,*b*-plane may change by up to 6 deg; assuming a radius of ~6 Å for the complex cation, such reorientations correspond to displacements of the peripheral hydrogen atoms again amounting to ~0.1 Å. These perturbations at or in the immediate environment of the $[Fe^{II}(2\text{-pic})_3]$ units are related to the cooperativity of spin crossover in a complicated way that does not seem to follow simple rules. The problem is best illustrated by reiterating the fact that in the isostructural series of $[Fe^{II}(2\text{-pic})_3]Cl_2$ solvates we have observed not only bi-stability, tri-stability and a range of transition temperatures, but also cases of complete suppression of spin conversion [6]. These results and especially the detailed findings described for the 2-propanol and ethanol solvates illustrate that cooperative transitions between two states in crystals built from bi-stable constituents are but the simplest among a multitude of possible scenarios, only some of which have been observed experimentally or predicted theoretically so far.

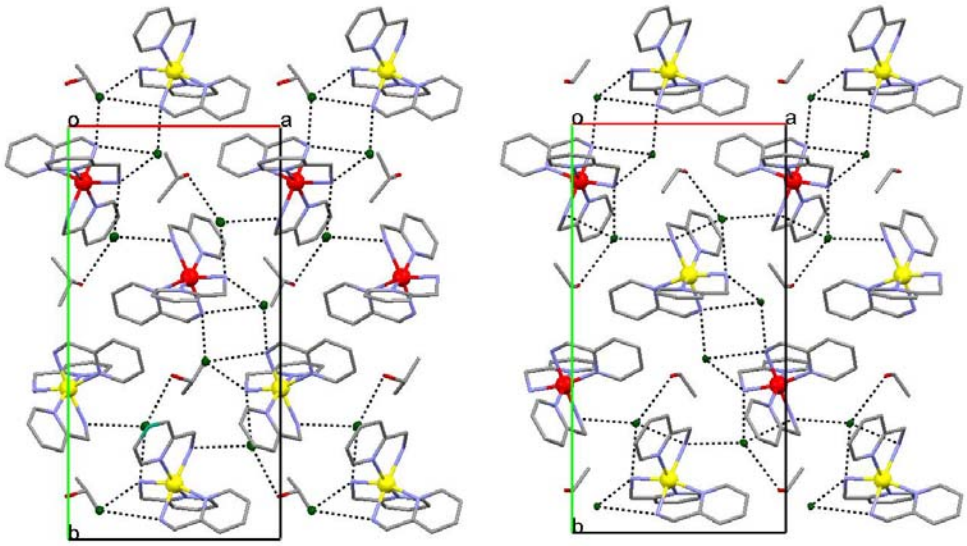

Fig. 1. Packing diagrams of $[Fe(2\text{-pic})_3]Cl_2 \cdot 2$-propanol (1, left) and of the corresponding ethanol solvate (right) in their intermediate phases. Note the different ordering patterns indicated by red (LS) and yellow iron atoms (HS). Chlorine atoms are shown as small green balls; dotted black lines indicate hydrogen bonding.

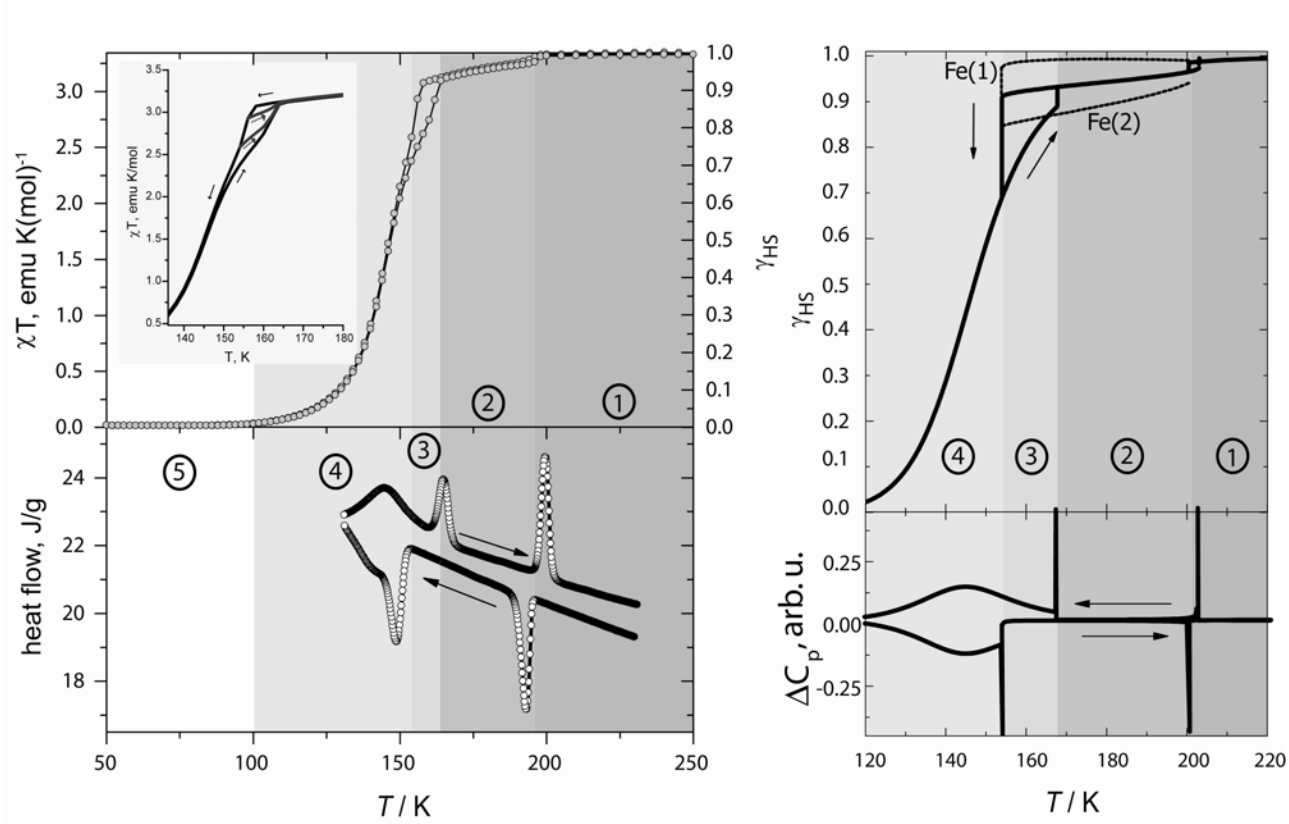

Fig. 2. Macroscopic properties of $[Fe^{II}(2\text{-pic})_3]Cl_2 \cdot 2$-propanol (1) as a function of temperature. The numbered grey zones indicate the following macroscopic regimes (see text): ① High-temperature phase, purely HS ② Intermediate HS phase (HS IP) ③ Hysteresis zone ④ Low-temperature phase, HS/LS zone ⑤ Low-temperature phase, purely LS
(Top left): χT from SQUID measurements, the insert shows inner hysteresis loops. - (Bottom left): heat flow as recorded by DSC for a heating and a cooling cycle. - *(Top right)*: HS fraction from a phenomenological model (see Ref. 4). The temperature dependence of the average HS fraction is shown as a bold solid line, the HS fractions of the two different iron sites within zone ② as thin dashed lines. - (Bottom right): specific heat from the model.

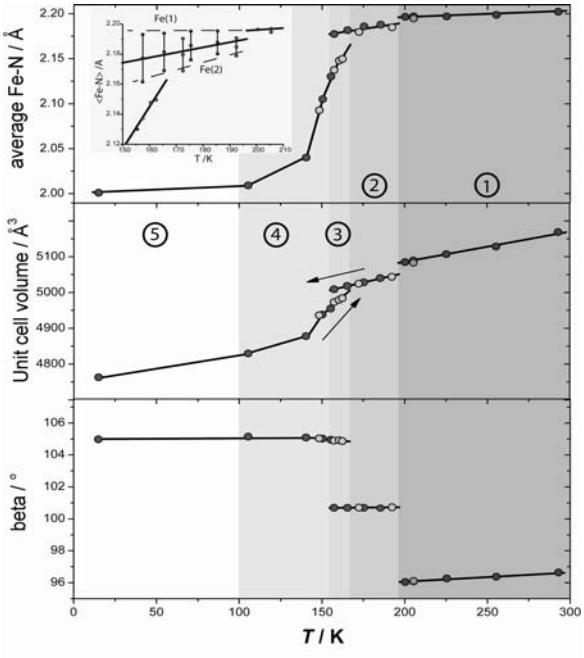

Fig. 3. Structural properties of $[Fe(2\text{-pic})_3]Cl_2 \cdot 2$-propanol, 1, as a function of temperature. - *(Top):* average iron-nitrogen bond lengths; the insert shows the overall average bond lengths and the separate averages for the two crystallographically non-equivalent iron complexes in the HS IP region ②. - (Middle): unit cell volume. - *(Bottom)*: the monoclinic angle undergoes two jumps at the first order transformations. - Dark-grey balls represent measurements from a cooling cycle, light-grey balls from a heating cycle. Solid lines are guides for the eye. The numbered grey zones have the same meaning as in Figure 2.

[1] P. Gütlich, Y. Garcia, H. Spiering in *Magnetism: Molecules to Materials IV* (Eds.: J. S. Miller, M. Drillon), Wiley-VCH, Weinheim, 2002, 271
[2} O. Kahn, C. J. Martinez, *Science* 1998, *279*, 44
[3] A. Bousseksou, G. C. Molnar, *C. R. Chimie* 2003, *6*, 1175
[4] K. W. Törnroos, M. Hostettler, D. Chernyshov, B. Vangdal, and H. B. Bürgi, Chemistry-A European Journal 2006, *12*, 6207
[5] D. Chernyshov, M. Hostettler, K.W. Törnroos, and H.-B. Bürgi, Angew. Chem. 115, 3955 (2003); Angew. Chem., Int. Ed. 2003, *42*, 3825
[6] M. Hostettler, K.W. Törnroos, D. Chernyshov, B. Vangdal, and H.-B. Bürgi, Angew. Chem. 116, 4689 (2004); Angew. Chem., Int. Ed. 2004, *43*, 4589

Metal-organic framework compounds with coordinatively unsaturated metal atoms for hydrogen storage

Pascal D. C. Dietzel[1,2], Richard Blom[2], and Helmer Fjellvåg[1]

[1]Centre of Materials Science and Nanotechnology, Department of Chemistry, University of Oslo; [2]SINTEF Materials and Chemistry

There is a strong interest in developing alternative energy sources because of the consequences ensuing from the continuous burning of fossil fuels. A potential solution is to use hydrogen, which has been produced by environmentally friendly processes as energy carrier. This poses new challenges regarding storage and transportation of hydrogen. Current research indicates that the amount of gas a given material may take up scales with its apparent surface area. One of the substance classes holding promise in this regard are coordination polymers, otherwise known as metal-organic frameworks (MOFs), whose extreme porosity is unique among substances with well-defined long range order. Unfortunately, cryogenic temperatures are necessary to store large amounts of hydrogen by physisorption to surfaces. Consequently, materials with an increased interaction between adsorbents and adsorbate are sought to increase the applicable temperature range. Metal cations with freely accessible coordination sites where the gas may adsorb are expected to result in such strong interactions.

As a consequence of their extended structures, MOF compounds are commonly highly crystalline, but they also exhibit a fairly low solubility. This often results in polycrystalline samples unsuitable for single-crystal diffraction experiments. Because the MOFs are predominantly composed of light atoms with weak scattering power, the observed intensity rapidly declines with theta, which is even more pronounced for highly porous structures. Many MOFs also have quite large unit cells. As a result of these issues, one frequently observes many overlapping reflections with low intensity already at modestly low theta values. This often already prevents indexation of the sample from common laboratory X-ray data, much less allowing for structure solution. Synchrotron radiation with its superior brilliance and angular resolution is perfectly suited to circumvent these problems.

Reaction of nickel(II) acetate and 2,5-dihydroxyterephthalic acid (H_4dhtp) in a THF-water mixture yields the substance, $Ni_2(dhtp)(H_2O)_2{\cdot}8H_2O$, whose crystallites are too small for single-crystal structure determination. The powder diffraction pattern, however, was very similar to the pattern of $Co_2(dhtp)(H_2O)_2{\cdot}8H_2O$, which we had investigated previously. Using the latter as structural model, we were able to determine the structure of the nickel compound by Rietveld refinement from data collected at the SNBL (Figure 1a). Indeed, both compounds are isostructural with a three-dimensional honeycomb-like network (Figure 2a).

The channels in the honeycomb have a diameter of ~11 Å, and they account for approximately 60% of the volume of the structure. After synthesis, these channels are filled with water. At the intersections of the honeycomb are

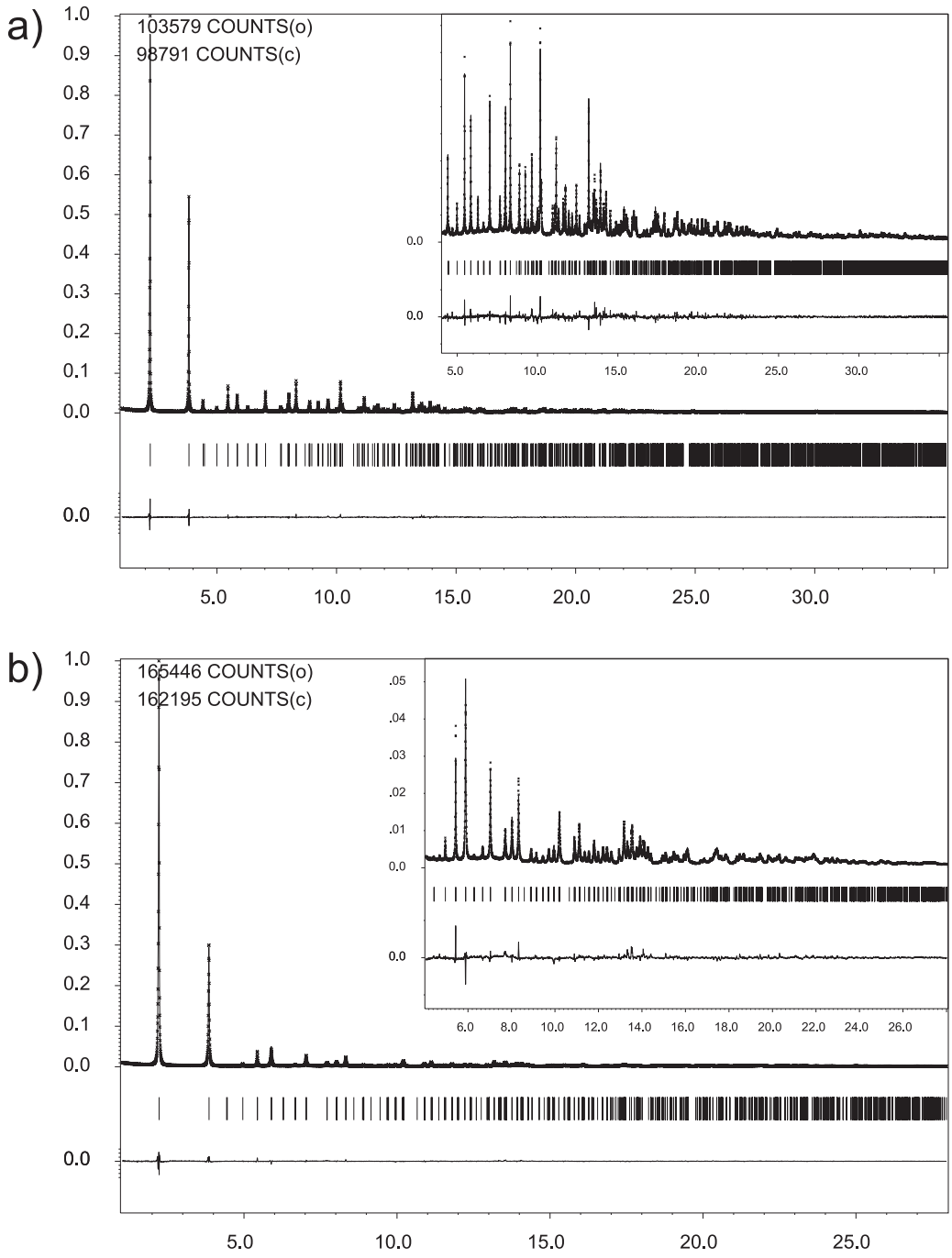

Fig. 1 Rietveld refinement plots of the hydrated (a) and dehydrated (b) form of $Ni_2(dhtp)(H_2O)_2 \cdot 8H_2O$ (crosses: observed pattern, line: calculated pattern, bottom line: difference plot, all plotted on the same scale. Bragg peaks are indicated by tick marks. Insets: enlarged view of the high angle range).

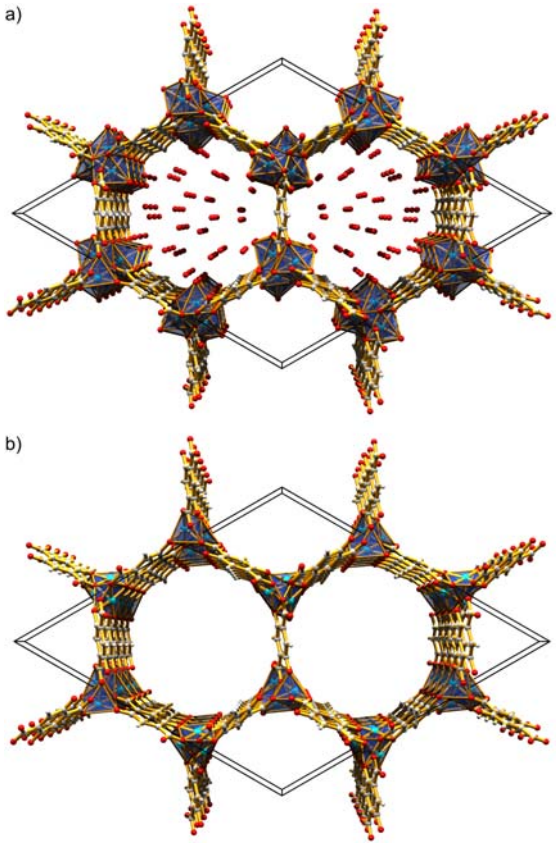

Fig. 2 Crystal structure of $Ni_2(dhtp)(H_2O)_2 \cdot 8H_2O$ in the hydrated (a) and dehydrated form (b). The vertices of the metal coordination octahedral, which point towards the cavities in (a) represent the metal coordinating water molecule. Notice their absence in (b).

helical chains of *cis*-edge connected nickel oxygen octahedra. One of the coordinating oxygen atoms of these octahedra belongs to a solvent water molecule which points towards the cavity. Consequently, it was decisive to establish the effect the removal of this water molecule has on the compounds stability and properties.

On heating, the solvent water is removed from the structure, and we have shown from thermodiffraction data that the framework remains stable in an inert atmosphere of nitrogen, while the crystalline phase disappears soon after we expect the final water to have been removed from the structure when the experiment is conducted in air. Dehydration and rehydration experiments in the TG confirmed that the ability of the substance to take up the identical amount of water that was removed on heating is correlated to the crystallinity of the substance.

The stability of the dehydrated compound in inert atmosphere opened up the possibility of determination of its structure. For this, a sample was desolvated *ex-situ* by filling it in a capillary and heating it in a dynamic vacuum under the inert conditions of a vacuum line. The capillary was flame-sealed and transported to the beamline in Grenoble, where high-resolution powder data were collected. Structure refinement (figure 1b) confirmed the absence of the water molecules in the channel and on the metal (Figure 2b), and allowed for a detailed comparison between the hydrated and dehydrated structure.

The permanent porosity of this compound is also demonstrated by the reversible uptake of nitrogen at 77 K. The nitrogen adsorption isotherm yields a Langmuir surface area, of 1083 $m^2\ g^{-1}$ and a pore volume of 0.41 $cm^3\ g^{-1}$. Apart from the high specific surface area an important factor for hydrogen adsorption in metal-organic frameworks is the presence of strong adsorption sites such as the open metal sites in the dehydrated nickel compound. The hydrogen adsorption isotherms, measured in collaboration with Barbara Panella and Michael Hirscher at the Max-Planck-Institute for Metals

Research in Germany, has a type I profile at 77 K, as expected for a microporous material, and it is independent of the number of adsorption cycles. This indicates that the hydrogen uptake is completely reversible, as expected for physisorption. The fit with a Langmuir equation yields a saturation value of 1.8 wt%. At room temperature and approximately 65 bar, the storage capacity is less than 0.3 wt% as is usual for physical adsorption at ambient conditions.

The absolute hydrogen storage capacity of this material is, unfortunately, not high enough for application in a commercial storage system. However, it is an ideal model system to study the interaction of hydrogen (and other adsorbents) with a porous material containing accessible metal sites.

Reference

P. D. C. Dietzel, B. Panella, M. Hirscher, R. Blom, H. Fjellvåg, “Hydrogen adsorption in a nickel based coordination polymer with open metal sites in the cylindrical cavities of the desolvated framework”, *Chem. Commun.* **2006**, 959-961.

$La_2MgNi_2H_8$, containing isolated $[Ni_2H_7]^{7-}$ and $[Ni_4H_{12}]^{12-}$ anions

Jean-Noël Chotard[1], Yaroslav Filinchuk[1,3], Bernard Revaz[2] and Klaus Yvon[1]

[1]Laboratoire de Cristallographie, Université de Genève
[2]Département de Physique de la Matière Condensée, Université de Genève
[3]Current address:Swiss Norwegian Beam Lines at ESRF,BP-220, 38043 Grenoble, France

Solid-state metal hydrides provide a safe and efficient way of storing hydrogen. Those forming metal – hydrogen "complexes" are of particular interest because they are associated with high storage efficiencies, great compositional and structural variety, and interesting properties, such as hydrogen induced metal-insulator transitions [1]. Among the known complexes, most are mononuclear and display terminal hydrogen (H) ligands. Polynuclear complexes displaying bridging H ligands are less common but of considerable interest because they provide possible links to "interstitial" hydrides. Following our discovery of a hydrogen induced insulating state in the $LaMg_2Ni$-H system [1], we have investigated the closely related La_2MgNi_2-H system and found a stoichiometric hydride of composition $La_2MgNi_2H_8$. The compound forms at 100°C and 30 bar hydrogen pressure and represents the first example of a solid–state metal hydride containing different types of polynuclear hydride complexes. In contrast to $LaMg_2NiH_7$, which displays mononuclear tetrahedral $[NiH_4]^{4-}$ complexes [1], $La_2MgNi_2H_8$ contains a fully ordered arrangement of isolated dinuclear $[Ni_2H_7]^{7-}$ (**I**) and tetranuclear $[Ni_4H_{12}]^{12-}$ (**II**) complexes (see figure 1). Interestingly, hydrogenation leaves the metal atom arrangement nearly unchanged and leads to a metal-insulator transition which is a relatively rare phenomenon in transition metal-hydrogen systems.

The structure was solved on the deuteride by using both synchrotron (Swiss–Norwegian beam line BM01) and neutron (HRPT, PSI Villigen) powder diffraction data, and refined by the Rietveld method. Synchrotron data showed a small monoclinic distortion of the tetragonal host structure and could be indexed in the centrosymmetric space group $P2_1/c$ by using the automatic indexing program DICVOL04 [2]. Among the 16 independent deuterium (D) atoms found by FOX [3], 13 are bonded to nickel and form the complexes **I** and **II**, while the remaining three are not bonded to nickel and occupy either tetrahedral $[La_2Mg_2]$ or octahedral $[La_4Mg_2]$ interstices in an essentially ionic environment. All Ni atoms have tetrahedral D atom configurations and display both terminal and bridging D ligands. As expected, the Ni-D distances of the terminal ligands are slightly shorter on the average (Ni-D=1.58 Å) than of the bridging ligands (Ni-D=1.61 Å), and compare well with those in other complex metal hydrides containing mononuclear NiD_4 complexes, such as $LaMg_2NiD_7$ (1.58 Å), Mg_2NiD_4 (1.54 Å) and $CaMgNiD_4$ (1.60 Å). Taken together, these structural features suggest the limiting ionic formula $4.La_2MgNi_2D_8 = La_8^{3+}Mg_4^{2+}[Ni_4D_{12}]^{12-}2.[Ni_2D_7]^{7-}6D^-$. In other words, the electron requirement of the transition element in each complex (**I**: 34, **II**: 64 electrons) can be rationalized in terms of the 18 electron rule by attributing 2-center two-electron bonds to terminal D atoms and 3-

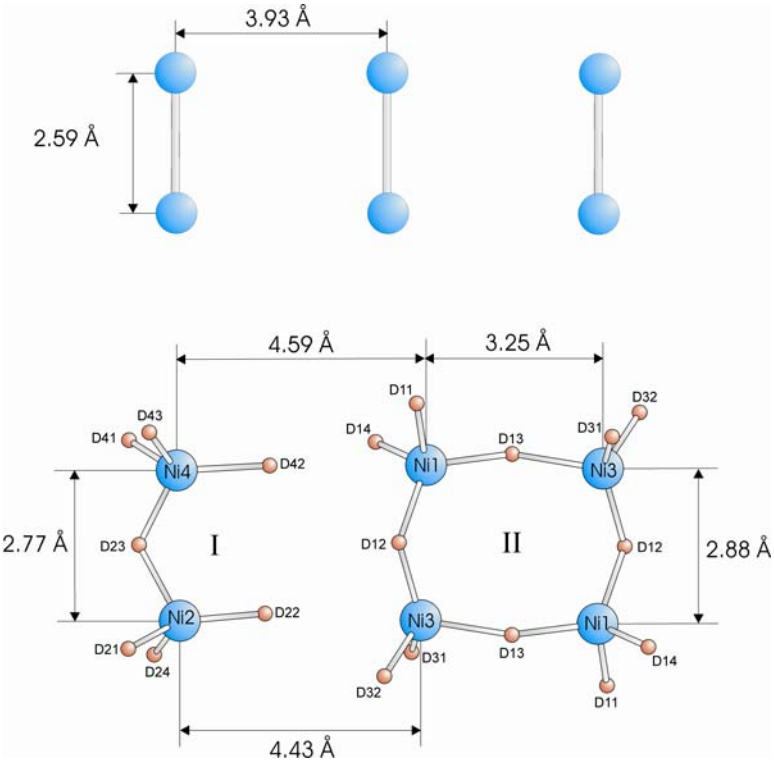

Figure 1: Dinuclear $[Ni_2D_7]$ (I) and tetranuclear $[Ni_4D_{12}]$ (II) complexes in $La_2MgNi_2D_8$ (bottom) and comparison with hydrogen free La_2MgNi_2 (top)

center 2-electron bonds to bridging D atoms. This model implies that Ni is essentially zero-valent, i.e. that the *d* bands are filled, and that the compound is diamagnetic and possibly insulating.

In order to test these assumptions, magnetic and electrical resistance measurements have been performed on hydride powders. While the results confirmed the expected semiconducting behaviour, they suggested slight ferromagnetism rather than the expected diamagnetism. This behaviour is probably due to traces of ferromagnetic nickel in samples of the intermetallic compound not detected by diffraction methods, and the formation of additional nickel at the grain boundaries during hydrogenation. The latter so-called 'surface segregation' effect has already been observed in related metal-hydrogen systems such as $LaNi_5$–H [4] and presumably masks the expected diamagnetism of $La_2MgNi_2H_8$.

Published in Angew. Chem. Int. Ed, **2006**, *45*, 7770

References:

[1] K. Yvon, G. Renaudin, C.M. Wei, M.Y. Chou, *Hydrogenation-Induced Insulating State in the Intermetallic Compound $LaMg_2Ni$.* Phys. Rev. Letters, 2005. 94(6): p. 066403-4.

[2] A. Boultif , D.L., *Dicvol04.* J. Appl. Crystallogr., 2004. 37: p. 724-731.

[3] V. Favre-Nicolin, R. Černy, J. Appl. Cryst., 2002. 35: p. 734-743.

[4] L.Schlapbach, *Magnetic properties of $LaNi_5$ and their variation with hydrogen absorption and desorption.* J. Phys. F: Metal Phys., 1980. 10: p. 2477-2490.

Structure-function studies of proteins from species adapted to extreme environments

Altermark, B., Brandsdal, B.O., Helland, R., Karlsen, S., Leiros, H.K.S., Leiros, I., Lorentzen, M.S., Moe, E., Niiranen, L., Os, V., Riise, E.K., Smalås, A.O., Willassen, N.P
(Tromsø, Norway)

Introduction

Organisms living at extreme temperatures are faced with the challenge of overcoming altered physiochemical properties induced by the temperature. Thermophiles live at temperatures where most proteins from mesophilic species will unfold rapidly, while at the other end of the temperature scale, the psychrophiles have to cope with reduced molecular motion, lower membrane fluidity, reduced turnover rate of enzymes and increased viscosity. Still, both thermophiles and psychrophiles maintain metabolic processes on a level comparable to organisms living at moderate temperatures. Although the vast majority of ecosystems on Earth are exposed to cold environments, like in Arctic, Antarctic and deep sea waters, and polar and alpine regions, most attention has, until recently, been given to proteins from organisms at the higher end of the temperature scale.
Enzymes possessing psychrophilic properties are generally characterized by a higher catalytic efficiency, suggested to be due to higher flexibility, at the expense of a lower thermal stability than their more temperate homologoues. The majority of the enzymes which has been used as model systems for psychrophile research has been extracellular and of marine origin. This means that the enzymes also are affected by the salinity of the surrounding environment. This poses a problem when conclusions about the mechanisms of cold adaptation are to be drawn. Are the observed adjustments a result of true adaptation to low temperature, or a combination of cold and salt adaptation? To address the issues of adaptation, two enzymes from the cold adapted fish pathogen bacterium *Vibrio salmonicida* have been chosen as model systems. Catalase is intracellular and is thus unaffected by salt, while Endonuclease I is extracellular and affected by salt.

CATALASE

The cold adapted catalase from the fish pathogen bacterium *V. salmonicida* (VSC) has recently been characterised and shown to be two times more catalytically efficient compared to catalase from the mesophilic human pathogen *Proteus mirabilis* (PMC). VSC is also less temperature stabile with a half life of 5 min compared to 50 min for PMC at 60°C. This was the driving force for solving the crystal structure of the cold adapted VSC (Fig. 1).
Catalase degrades the near diffusion controlled decomposition of hydrogen peroxide into water and molecular oxygen, and function as a protective response to damage of cellular components. The active site includes His54 and Asn127 on the distal side of the important heme

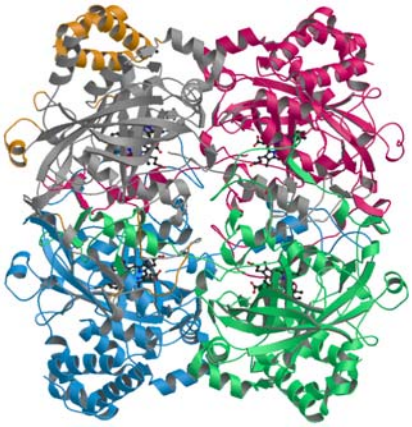

Figure 1 Ribbon figure of the tetrameric structure of catalase from *V. salmonicida*. Each of the four monomers (coloured gray and orange (monomer A), red, blue and green) contains an active site including a heme group (ball-and-stick models).

group, and Tyr337 on the proximal side of the heme (Fig. 2). From the molecular surface to the active site, there is a funnel shaped channel, the major channel, of approximately 30 Å, that allows access of substrate to the heme group (Fig. 3).

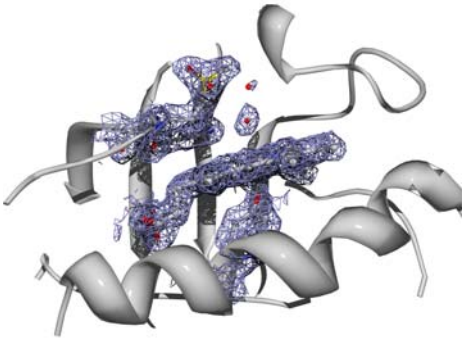

Figure 2 The heme-group, Met*53, His54, Tyr336 and two waters with $2F_oF_c$-electron density at 2.0σ of VSC.

Our results show that the increased catalytic efficiency of VSC could be due to smaller sized residues and reduced number of hydrogen bonds in the heme binding site. Also, increased channel diameter and fewer ion-pair interactions and hydrogen bonds within the major channel may provide the substrate with easier access to the active site and to the heme group in VSC than in PMC.

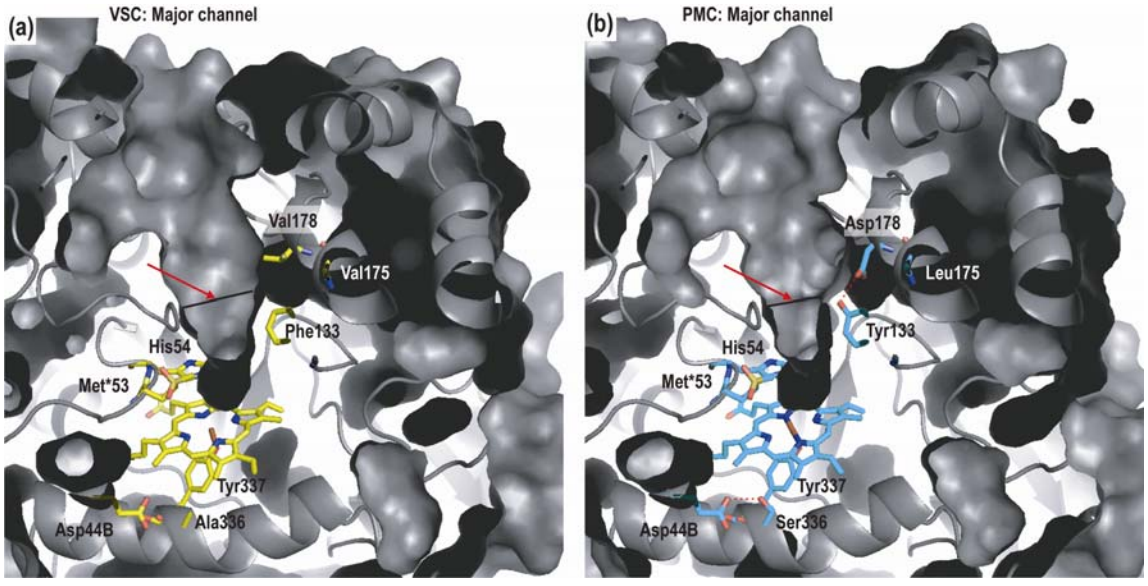

Figure 3 The major channel in VSC (a) compared to PMC (b) where dissimilar residues are shown.

Possible explanations for the lower thermal stability of VSC are slightly lower number of ion-pairs in the monomers and fewer residues involved in ion-pair networks. One VSC tetramer seems to be slightly more stabilized by intersubunit ion-pair interactions than in PMC, and to our knowledge a reduced number of intradomain electrostatic interactions combined with a higher number of intersubunit ion-pair interactions have not previously been observed in other cold adapted enzymes. The most important factor is perhaps the missing ion-pair interactions from C-terminal helices (α9-α12) to the rest of the molecule, this helix bundle is displaced in VSC relative to PMC as observed in the crystal structures, and since they include the C-terminus of the protein, this could be an unfolding site in VSC.

ENDONUCLEASE I

Endonuclease I (EndA, Fig. 4) is an extracellular enzyme where the exact function is unknown, but it has been suggested to be involved in the pathogenicity of the bacteria by degradation of nucleic acids in the host mucus layer, and hence, reducing the viscosity through which the bacterium has to pass.

EndA from two *Vibrio* species, the cold adapted and halotolerant *V. salmonicida* (*Vs*EndA) and the temperate *V. cholerae* (*Vc*EndA) were compared biochemically with respect to adaptation to temperature and adaptation to salt. It was found that optimum activity of the two enzymes correlated well with the external growth environment of the bacteria where *Vs*EndA has an activity optimum at much higher salt concentration than *Vc*EndA (Fig 5A), and it was also found that the cold adapted enzyme has lower temperature stability than *Vc*EndA (Fig 5B).

The electrostatic surface potential of the cold adapted enzyme is significantly more positive (blue regions, Fig 6 A and C) than the temperate enzyme due to a higher number of Lys residues, something which would favour substrate binding. However, when calculating the surface potential at the respective salt optimum concentrations, the potentials become surprisingly similar (Fig 6B and D).

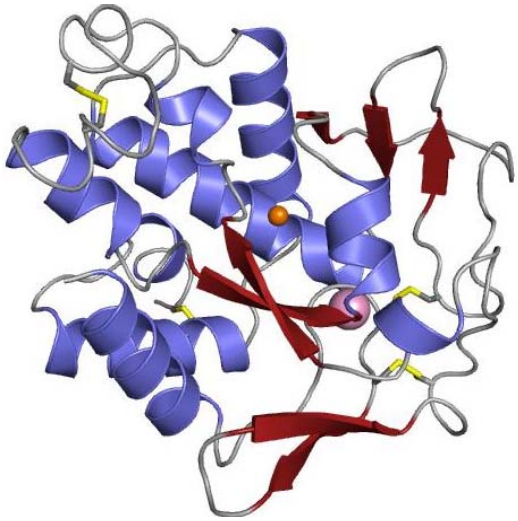

Figure 4 Ribbon figure of *Vs*EndA. The active site Mg^{2+} is shown in orange and the buried Cl^- in pink.

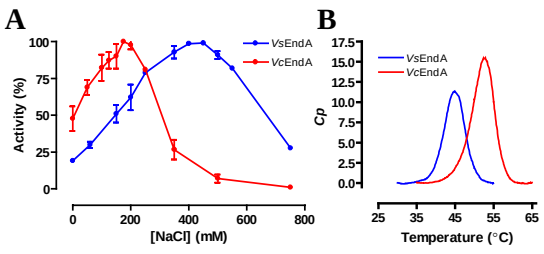

Figure 5 A) Activity versus NaCl concentration. B) Thermal denaturation measured by differential scanning calorimetry. *Vs*EndA is drawn in blue and *Vc*EndA in red line.

A, *Vs*EndA **B,** *Vs*EndA

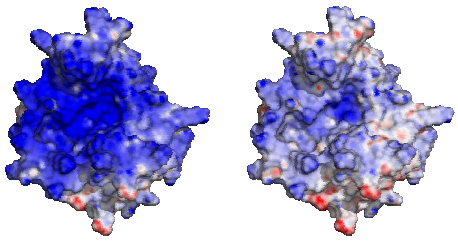

C, *Vc*EndA **D,** *Vc*EndA

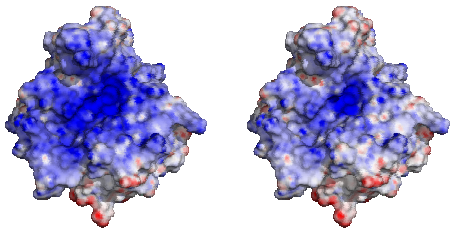

Figure 6 Electrostatic surface potential of *Vs*EndA and *Vc*EndA calculated with and without NaCl. (A) *Vs*EndA without NaCl and (B) with 425 mM NaCl. (C) *Vc*EndA without NaCl and (D) with 175 mM NaCl.

The increase in the number of Lys in *Vs*EndA is therefore suggested to have adaptational purposes both towards temperature and salinity. A more positively charged surface would favour substrate affinity, but unspecific binding of NaCl to the surface would prevent too strong interactions between the enzyme and the substrate and products. Placing the charged Lys residues close in 3D space would destabilize the enzyme and provide the protein with sufficient flexibility for efficient catalysis in a cold, saline environment.

Acknowledgement

The structure-function analysis of Catalase described above is based on our X-ray data to 1.96 Å collected at SNBL and on PDB entry 1M85. The structural comparison of Endonuclease I is based on our X-ray data collected to 1.6 Å at SNBL (*Vc*EndA) and 1.5 Å at ID29 (*Vs*EndA).

References

Altermark, B., Smalås, A.O., Willassen, N.P. and Helland, R. (2006). "*The structure of Vibrio cholerae extracellular endonuclease I reveals the presence of a buried chloride ion.*" *Acta Cryst.* **D62**, 1387-91

Altermark, B., Niiranen, L., Willassen, N.P., Smalås, A.O., and Moe, E. (2007). "*Comparative studies of endonuclease I from cold adapted Vibrio salmonicida and mesophilic Vibrio cholerae.*" FEBS Journal. **274**, 252-263.

Lorentzen, M.S., Moe, E., Jouve, H. and Willassen, N.P. (2006). "*Cold adapted features of Vibrio salmonicida catalase. Characterisation and comparison to the mesophilic counterpart from Proteus mirabilis.*"Extremophiles, **10**, 427-440.

Riise, E. K., Lorentzen, M. S., Helland, R., Smalås, A.O., Leiros, H-K. and Willassen, N. P. (2007) "*The first crystal structure of a cold active catalase from Vibrio salmonicida at 1.96 Å reveals structural aspects of cold adaptation*" Acta Cryst. **D63**, 135-148.

Altermark, B., Helland, R., Moe, E., Willassen, N.P. and Smalås, A.O. (2007) Structural adaptation of endonuclease I from the cold-adapted and halophilic bacterium *Vibrio salmonicida*. In preparation

Combination of *in situ* EXAFS and XRD with on-line gas analysis during the total oxidation of methane over palladium based catalysts

Jan-Dierk Grunwaldt, Niels van Vegten, Alfons Baiker
(Department of Chemistry and Applied Biosciences, ETH Zürich)

Palladium-based catalysts are regarded the most active materials in the total combustion of methane under lean burn conditions [1,2]. They are applied in exhaust catalytic converter systems and find use in gas turbines. We have recently found that Pd/Al_2O_3 and Pd/ZrO_2 catalysts prepared by flame-spray pyrolysis exhibit a high catalytic activity [3,4]. However, the mechanism for methane oxidation is complex [1,2], and not yet completely understood. In particular, a characteristic hysteresis in reaction rates is observed during heating up and cooling down in a methane/oxygen reaction mixture.

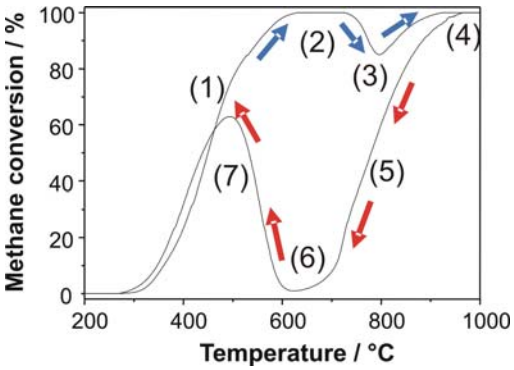

Fig. 1 Typical hysteresis in methane conversion over $10\%Pd/Al_2O_3$ in $1\%CH_4/4\%O_2$ in He [3]; the different steps marked on the lines are referred to in the text.

Figure 1 shows a typical cycle during heating up (steps 1 to 4) and cooling down over Pd/Al_2O_3 (4 to 7). The deactivation step 3 is speculated to be connected to a decomposition of PdO to metallic Pd [1]. However, metallic Pd is known to be very active in methane oxidation as well [5]. In order to elucidate the oxidation state of the Pd-particles under reaction conditions, *in situ* spectroscopy is required. This information may allow correlating the catalytic activity during the heating-cooling cycle with the structure of the catalysts.

For this purpose, the high temperature oven of SNBL combined with a capillary cell was used (setup similar to [3]). As Figure 1 demonstrates, the temperature was cycled between room temperature and 900 °C. Since the Pd-particles were not visible by XRD despite the high concentration in a $10\%Pd/ZrO_2$ catalyst, mainly X-ray absorption spectroscopy was applied. In order to gain insight into possible sintering of the Pd particles, the catalyst was additionally investigated by XRD at selected temperatures.

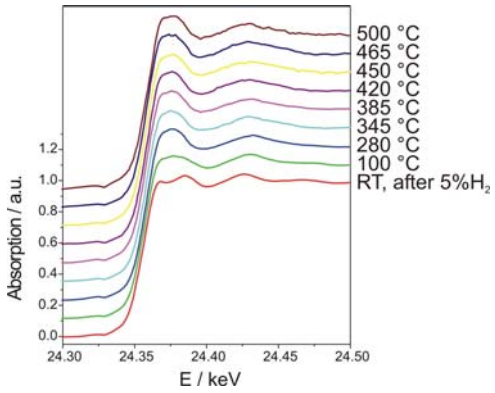

Fig. 2 XANES spectra at the Pd K-edge during the methane combustion over $10\%Pd/ZrO_2$ in $1\%CH_4/4\%O_2$/He; in parallel on-line catalytic data (Fig. 3) and XRD data (Fig. 4) were recorded.

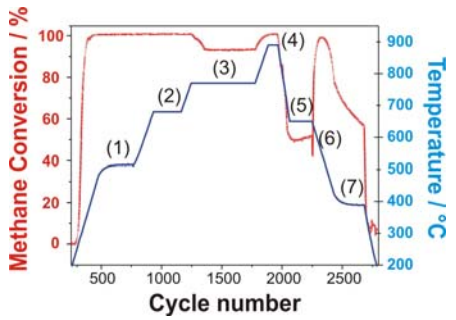

Fig. 3 Methane conversion (red) as function of temperature (blue) during the the methane combustion over 10%Pd/ZrO_2 in 1%CH_4/4%O_2/He; the steps correspond to this in Fig. 1.

Figure 2 shows XANES spectra during heating to 500 °C. Since it was previously found that a pre-reduced catalyst exhibits a higher reaction rate [2], the catalyst was mildly reduced beforehand. The catalysts behaved very similar to the one in Figure 1 and also the on-line catalytic data in Figure 3 show the ignition of the catalytic combustion of methane already below 500 °C. Under these conditions, the palladium constituent was re-oxidized. In XRD neither oxidic nor metallic palladium related reflections were found, indicating that the palladium is highly dispersed (Fig. 4).

When further heating to 770 °C (Fig. 5), the catalyst remained predominantly in oxidized state and the methane conversion stayed high (cf. Fig. 3) but at 770 °C it dropped. At the same time metallic Pd appeared both in the XAS spectra (Fig. 5) and the XRD patterns (Fig. 4). This implies that metallic Pd forms at high temperatures and, in parallel, a strong sintering of the Pd particles occurs. Both effects seem to lead to a drop in activity as observed in the on-line catalytic

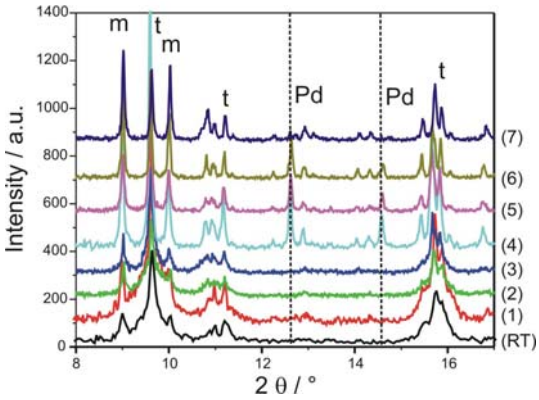

Fig. 4 XRD pattern during methane combustion over 10%Pd/ZrO_2 in 1%CH_4/4%O_2/He; RT: after reduction in 5%H_2/He; (1) 150 °C, (2) 500 °C, (3) 670 °C, (4) 770 °C, (5) after 890 °C down to 770°C, (6) 630 °C, and (7) 400°C.

data in Figure 3 corresponding to the effect observed in step 3 in Figure 1. During further heating to 900 °C, the palladium constituent remained in metallic state and the catalytic activity increased again, probably due to a different oxidation mechanism (homogeneous gas phase reaction).

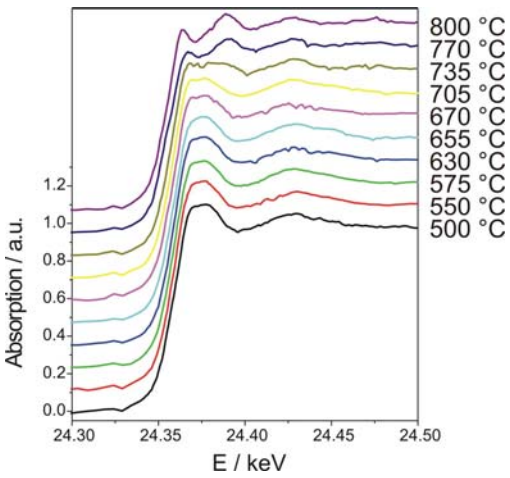

Fig. 5 XANES spectra at the Pd K-edge during the methane combustion over 10%Pd/ZrO_2 in 1%CH_4/4%O_2/He; in parallel on-line catalytic data (Fig. 3) and XRD data (Fig. 4) were recorded.

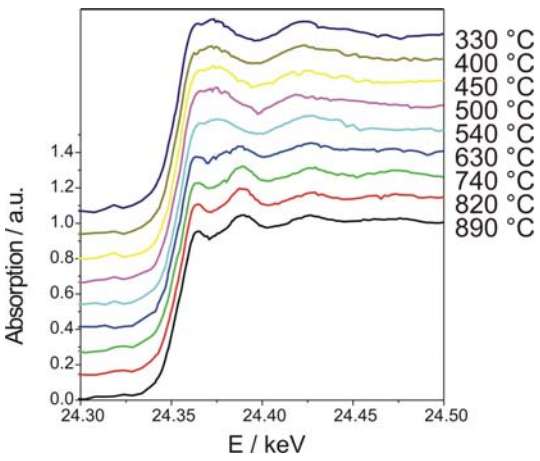

Fig. 6 XANES spectra at the Pd K-edge during the methane combustion over 10%Pd/ZrO_2 in 1%CH_4/4%O_2/He (cooling down of the catalyst in the reaction mixture); in parallel on-line catalytic data (Fig. 3) and XRD data (Fig. 4) were recorded.

During cooling down, the on-line catalytic data in Figure 3 demonstrate a similar hysteresis as shown in Figure 1 (step 6). The data both from XRD and Pd K-XANES reveal that palladium remains in metallic state. Only at significantly lower temperatures (below 600 °C, step 7), the palladium re-oxidizes and the catalytic activity increases again.

In summary, *operando* XAS and XRD data during the catalytic partial oxidation of methane were collected. They show a direct correlation between the structure and the performance of the catalyst. A strong deactivation is observed during thermal reduction of the catalyst accompanied by a sintering of the Pd particles. To our knowledge, this is the first *in situ* XAS/XRD study at high temperature combined with on-line catalytic data. It demonstrates the potential for parallel EXAFS and XRD analysis under reaction conditions, as well as the importance of measuring both the catalytic performance and the structure of the catalyst at the same time for deriving structure-performance relationships.

References

[1] D. Ciuparu, M. R. Lyubovsky, E. Altman, L. D. Pfefferle and A. Datye *Catalytic combustion of methane over palladium-based catalysts* CATAL. REV. SCI. ENG. **5** (2003) 1481.

[2] J.-D. Grunwaldt, M. Maciejewski and A. Baiker I*n situ X-ray absorption study during methane combustion over Pd/ZrO_2 catalysts* PHYS. CHEM. CHEM. PHYS. **5** (2003) 1481.

[3] J.-D. Grunwaldt, M. Caravati, S. Hannemann and A. Baiker *X-ray Absorption Spectroscopy under Reaction Conditions - Opportunities and Limitations of in situ Monitoring and Time-Resolved Studies of Heterogeneous Catalysts* PHYS. CHEM. CHEM. PHYS. **6** (2004) 3037.

[4] R. Strobel, J.-D. Grunwaldt, A. Camenzind, S. E. Pratsinis and A. Baiker *Flame-made Alumina-supported Pt-Pd particles and their Behaviour in Catalytic Methane Combustion* CATAL. LETT. **104** (2005) 9.

[5] M. Lyobovski and L. Pfefferle *Complete methane oxidation over Pd catalyst supported on alpha-alumina* CATAL. TODAY **47** (1999) 29

XAS characterisation of catalysts for fuel production

Magnus Rønning, Nina Hammer, Øyvind Borg, De Chen

Norwegian University of Science and Technology, NTNU
Department of Chemical Engineering,
N-7491 Trondheim, Norway

Identification of cobalt species during temperature programmed reduction of Fischer-Tropsch catalysts

Cobalt is considered to be the most favourable metal for the synthesis of long-chain hydrocarbons from natural gas-based synthesis gas because of its high activity, high selectivity to linear paraffins, high resistance towards deactivation, and low water-gas shift activity.

In order to maximise the exposure of cobalt to gaseous reactants, the metal is normally dispersed on a high surface area support. The choice of support is important for the final Fischer-Tropsch synthesis catalyst. In particular, the pore characteristics of the support have a significant effect on the Co_3O_4 crystallite size measured after impregnation and calcination. In some cases, the support interacts strongly with the active phase. Metal-support interactions may leave a fraction of the cobalt chemically inactive after reduction. In order to reduce the amount of non-reduced cobalt, a small amount of a second metal (Re, Pt) can be introduced into the catalyst system.

Temperature programmed reduction (TPR) is a valuable method for gathering information about the reduction process. The reduction properties of cobalt oxide deposited on different support materials have been extensively investigated. Unsupported, as well as supported Co_3O_4, are reduced to cobalt metal in two-steps;

$$Co_3O_4 + H_2 \rightarrow 3CoO + H_2O$$

$$3CoO + 3H_2 \rightarrow 3Co + 3H_2O$$

X-ray absorption spectroscopy (XAS) can give information about the nature and quantity of different cobalt species present during reduction. For supported cobalt, these species usually include Co_3O_4, CoO, and metallic cobalt. In addition, a part of the cobalt may interact with the support, making complete reduction difficult. XAS can conveniently be performed *in situ* with the possibility to follow the dynamics of the process.

Several *in situ* cells have been used for studying the catalyst materials. An example of a versatile cell is shown below. The cell allows for combining techniques such as XAS, XRD and Raman by selecting appropriate window materials (Kapton or glassy carbon for X-rays, suprasil or sapphire for Raman).

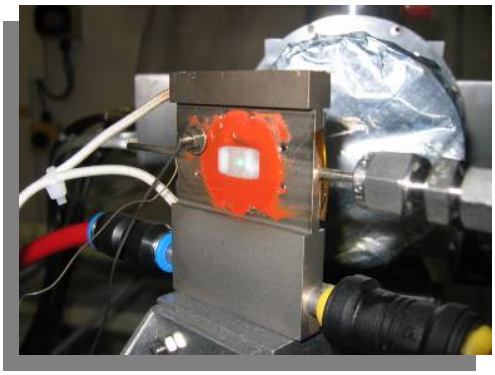

Figure 1. A versatile *in situ* catalysis cell that allows for combined measurements of XAS, XRD and Raman.

The degree of reduction ranges from 63 to 85 percent using linear combination of XANES profiles, while EXAFS analysis yields values from 65 to 79 percent. The consistency between values obtained from XANES profiles and EXAFS analysis is good and within experimental errors. The extent of reduction obtained by the XAS techniques follows the order $CoRe/SiO_2$ > $CoRe/TiO_2$ > $CoRe/\alpha$-Al_2O_3 > $CoRe/\gamma$-Al_2O_3.

XANES experiments at the Co K absorption edge were recorded during *in situ* reduction. According to a principal component analysis of the spectra, three primary components were needed to adequately reconstruct the spectra of all catalysts. Co_3O_4, CoO, and Co metal foil were chosen as model compounds.

An example of the change in XANES profiles during reduction of $12CoRe/\gamma$-Al_2O_3 is shown in Figure 2. The pre-edge feature typical for Co in partially tetrahedral coordination, which is the case for bulk Co_3O_4, gradually decreases. This change is consistent with the transformation to octahedrally coordinated Co as in CoO. Finally, the profiles closely resemble that of metallic Co showing a less intense white line and a characteristic pre-edge shoulder.

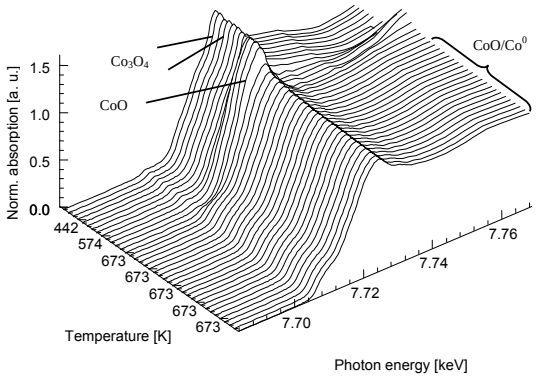

Figure 2. XANES profiles at different reduction stages for $CoRe/\gamma$-Al_2O_3. Scans were taken continuously with a time gap of five minutes.

Figure 3 display changes in Co_3O_4, CoO and Co metal fractions with temperature for the catalyst $CoRe/\gamma$-Al_2O_3. The shape of the component fraction plots for the other catalysts was similar to the catalyst presented here. The only significant differences for the various catalysts are the extent of reduction and the temperature in which the major transformation from Co_3O_4 to CoO occurs. For all catalysts the initial quantity of Co_3O_4 was completely transformed into other cobalt species before reaching the final reduction temperature of 673 K. Furthermore, CoO is the dominant intermediate during reduction for all supported cobalt catalysts included in this investigation.

The temperature for maximum CoO concentration coincides well with the temperature of the TPR peaks previously attributed to the reduction of Co_3O_4 to CoO. The XAS and TPR results are in agreement for the further reduction of cobalt, namely the reduction of CoO to cobalt metal. According to TPR, the reduction of CoO starts immediately after the reduction of Co_3O_4 is completed. The XAS results show an immediate rise in the cobalt metal content (Fig. 3).

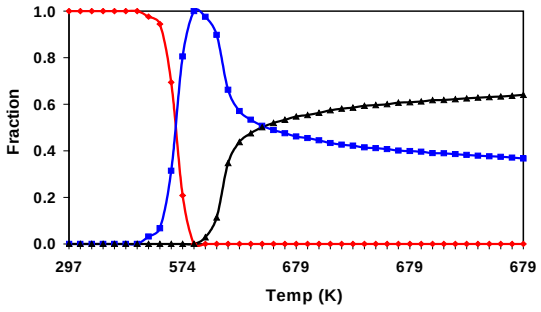

Figure 3. Temperature programmed reduction of $CoRe/\gamma$-Al_2O_3 using the *in situ* XAS cell. Temperature ramping is indicated in the figure (Red = Co_3O_4, Blue = CoO, Black = cobalt metal).

The linear combination of XANES and the principal component analysis give a very good fit to the experimental data.
In agreement with TPR and O_2 titration data, the degree of reduction was significantly higher for catalysts with high surface area than for the catalysts with low surface area. The degree of reduction was 70 % and 22 % after 3.5 h respectively. The degree of reduction did not change when the catalyst was exposed to synthesis gas. Thus, no oxidation of Co, which is a likely source for deactivation, occurred at the applied experimental conditions.

The results show that the XANES is capable of identifying the different cobalt species during the reduction. Linear combination of XANES profiles with those of selected reference compounds gives a relatively precise estimate of the extent of reduction of the cobalt particles.

Au-TiO_2 catalysts for the water-gas shift reaction stabilised by carbon nanofibres

The water-gas shift (WGS) reaction may provide a pathway to suppress the CO levels in the production of pure hydrogen for fuel-cell power systems. Gold nanoparticles in association with partially reducible oxides have been shown to exhibit high catalytic activity in the reaction. Carbon nanofibres (CNF) have been used in the present work to disperse and stabilise the TiO_2 support and hence the Au particles. The use of CNF as support material in heterogeneous catalysis has attracted growing interest due to their specific characteristics. The CNF are resistant to acid/base media and the precious metals can easily be recovered by burning off the support. The size and morphology of the CNF provide high surface areas while maintaining macroscopic pore sizes and hence good transport properties in the reactor, and reduced risk of micropore-induced diffusion limitations. The scope of the present work is to examine how the physical and chemical properties of the Au particles are influenced by the choice of support material and synthesis methods. The catalysts have been studied by various characterisation techniques and tested in the WGS reaction. The changes in the structure of Au and TiO_2 for different pre-treatments have been investigated by X-ray absorption spectroscopy. The Au catalysts have been prepared by deposition-precipitation and deposition of Au from colloid solutions on different supports. The supports used are TiO_2, CNF, and TiO_2 deposited on CNF. The results show that the properties obtained from the synthesis methods are highly dependent on the choice of support material.

XANES provides information about the oxidation states and site symmetries of the gold species. An *in situ* XAS study of the pre-treatment of the samples was performed. Linear combination of the edge profiles was performed using Au(0) (Au metal) and Au(I) (AuCl) as reference compounds to determine the distribution of valence states in the catalysts. No evidence of Au(III) could be detected in any of the samples before or during the different treatments. The changes in valence states for the Au catalysts are similar in oxygen and helium. Since the fraction of metallic Au is increasing with the same fraction in both gases it is likely that the changes observed are because of structural changes and

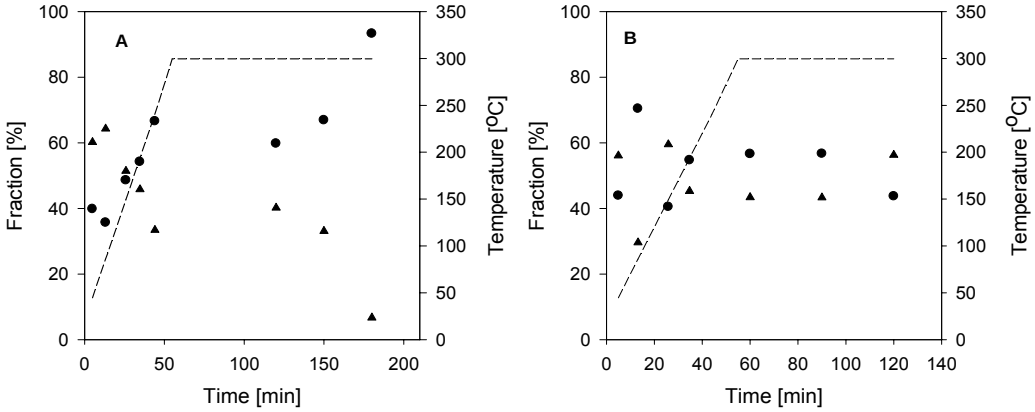

Figure 4: Fractions of Au(0) (circle) and Au(I) (triangles) obtained from linear combination of XANES spectra during different pre-treatments of $AuTiO_2CNF\_Col$, (A) treated in 5% O_2/He followed by (B) reduction in 5% H_2/He. The temperature is plotted as a dashed line.

rearrangements of the cluster-support induced by the thermal treatment. Since only Au(0) and Au(I) can be observed, oxidation of gold particles is not a likely explanation for the valence shift in the present samples. Others have reported EXAFS and XANES experiments and DFT calculations are suggesting a model where a metallic gold cluster containing about 50 atoms is in intimate contact with the oxide support, to the extent that up to 15 % of the gold atoms at the interface with the support may be located at cation vacancies. Such gold atoms would be expected to carry a small positive charge. This is in agreement with the positive charge that is observed in the XANES spectra being a result of gold-support interactions. However, it is clear that metallic gold is the main constituent in the samples from both synthesis methods.

The fraction of Au(I) is larger for $AuTiO_2$/CNF than for Au/CNF. This is because the average particle size is smaller for $AuTiO_2$/CNF, whereby a larger fraction of atoms is located at the metal-support interface where cationic gold is stabilised by the support. This indicates that titania has a stronger interaction with the Au particles than carbon. However, during heating in oxygen, the fraction of metallic gold in $AuTiO_2$/CNF increases as well and after two hours the total fraction of Au(0) is larger than for Au/CNF. Purging the sample in helium followed by introduction of H_2/He immediately results in changes in the fraction of Au(I). The fraction of Au(I) increases to approximately 45 % and is relatively constant during the treatment, see Figure 4. The relatively large change in oxidation states for Au can be a combination of structural changes and adsorption of hydrogen on the surface. Note that the Au(I) fraction is merely an expression of the partial positive charge on the Au atoms ($Au^{\delta+}$) rather than of a formal oxidation state.

In situ XAS studies show that the WGS activity is higher when the fraction of $Au^{\delta+}$ is high, although the positive charge during water-gas shift (WGS may) arise from CO (or hydrogen) chemisorption on Au or by dynamic changes in the metal-support interaction. Since titania is a partially reducible oxide, hydrogen may create vacancies in the oxide structure that are able to promote the interaction with gold particles.

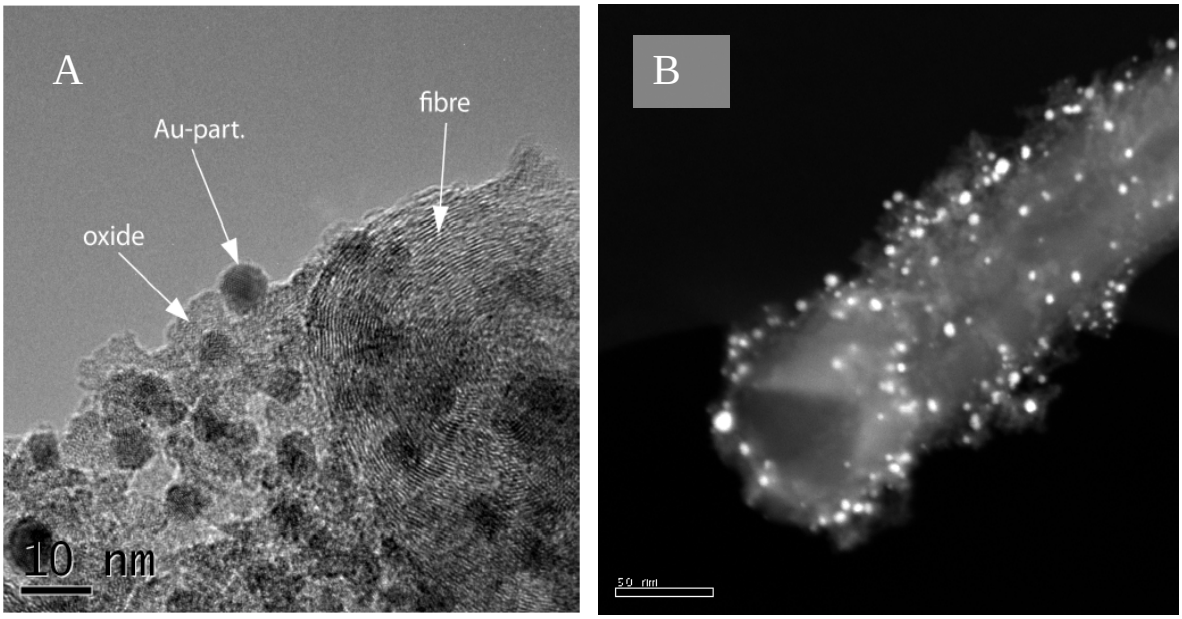

Figure 5. (A) TEM and (B) STEM images of the samples as-prepared showing Au particles selectively deposited on titania supported on CNF for $AuTiO_2CNF$.

The Au-Au coordination number increases after thermal treatment in oxygen and helium. However, the increase in coordination number is less pronounced for samples containing CNF. Oxidation followed by reduction of $AuTiO_2$/CNF causes no further increase in coordination number and the Au-Au interatomic distance. This suggests that the oxygen treatment leads to stronger interaction between the gold particles and the TiO_2 and prevents further particle sintering.

The WGS activity significantly improves when titania is present in the catalytic material compared to deposition of Au directly on CNF. This shows that high catalytic activity in the water-gas shift reaction is obtained only when both Au and the oxide are present, indicating that the active sites are either on the Au-TiO_2 interface or that the reaction follows a bifunctional mechanism. The specific rate is 8 times higher for the catalyst prepared by deposition-precipitation which indicates that residue from the colloid preparation has a detrimental effect on the catalytic activity and that the two preparation methods require different pre-treatment procedures to obtain high activity.

References

1. Ø. Borg, M. Rønning, S. Storsæter, W.van Beek, A. Holmen, Identification of cobalt species during temperature programmed reduction of Fischer-Tropsch catalysts, *Stud. Surf. Sci. Catal. 163 (2006), 255*

2. Ø. Borg, N Hammer, S. Eri, O.A. Lindvåg, R. Myrstad, E.A. Blekkan, M. Rønning, E. Rytter, A. Holmen, Fischer-Tropsch synthesis over un-promoted and Re-promoted γ-Al2O3 supported cobalt catalysts with different pore sizes, submitted to *Applied Catalysis A*

3. N. Hammer, I. Kvande, V. Gunnarsson, B. Tøtdal, X. Xu, D. Chen, M. Rønning, Au-TiO_2 Catalysts on Carbon Nanofibres Prepared by Deposition-Precipitation and from Colloid Solutions, *Catal. Today (2007), in press*

4. N. Hammer, I. Kvande, D. Chen, W. van Beek, M. Rønning, Identification of valence shifts in Au during the water-gas shift reaction, *Topics in Catalysis, (2007), in press*

5. N. Hammer, I. Kvande, D. Chen, M. Rønning: Au-TiO_2 catalysts stabilised by carbon nanofibres *Catal. Today (2007), in press*

6. F. Huber, Z. Yu, S. Lögdberg, M. Rønning, D. Chen, H. Venvik, A. Holmen, Remarks on the passivation of reduced Cu-, Ni-, Fe-, Co-based catalysts, *Catal. Lett. 110(3,4) (2006) 211*

7. M. Rønning, F. Huber, H. Meland, H. Venvik, D. Chen, A. Holmen, Relating catalyst structure and composition to the water-gas shift activity of Cu-Zn based mixed-oxide catalysts, *Catalysis Today, 100 (2005) 249-254*

STATUS OF FACILITY

BM1A: SINGLE CRYSTAL DIFFRACTOMETER AND LARGE AREA DETECTOR

P. Pattison

The last two years of operation on BM1A has been a period of consolidation rather than development, with the primary goal being to exploit in an optimal fashion the existing facilities on the beamline. There have been no major disturbances to the routine schedule of user operation, and the scientific throughput has been continuously improving. There has been a marked increase in the number and the complexity of *in-situ* experiments. For this reason, the improvement in the staffing of the beamline during this period has been a vital development. We have now reached the level of three full-time staff (beamline scientist, second scientist and postdoc, together with specialist support in the field of high pressure experiments).

We have recently passed the significant milestone of 100 publications which have appeared in the field of protein crystallography using data from SNBL. Many of these publications appeared in high impact journals (2 in *Nature*, 1 in *Science*, and 6 in *Structure,* for example), and it is impressive to see the quality of the science in this field which can emerge from a standard ESRF bending magnet beamline. At its peak, about 30% of the publications from BM1A were related to protein crystallography. Since the PX beamlines at the Swiss Light Source have come on-line, the fraction has remained steady at about 15%.

There has been an increase in the demand for materials science experiments at BM1A. In particular, this type of experiment can benefit from the possibilities for rapid, high quality powder diffraction data collection using the MAR345 image plate detector. Although the angular resolution which can be achieved with the area detector does not compare to the excellent line widths observed with the crystal analyzer set-up on BM1B, the resolution is still adequate for many scientific tasks. It is interesting to note that the angular resolution available with the MAR345 is competitive with most powder neutron diffractometers world-wide. In addition, the high sensitivity and efficiency of the image plate implies that challenging experiments such as high pressure diamond-anvil cell work can be successfully carried out even on a bending magnet source. The high pressure projects on BM1A currently produce about 20% of the total publications, and the trend is towards increasing demand for beamtime in this field.

The most dramatic development during the period 2005-2006 on BM1A has been the increased use of the image plate for investigating in-situ chemical reactions and phase transitions in powders. A successful SNBL demonstration experiment published in Journal of Synchrotron Radiation several years ago entitled *Characterization of complex phase transitions using powder diffraction and an area detector* [1] has led to a real boom in the popularity of this technique. This sudden increase has partly been driven by the immense significance of *in-situ* experiments for characterizing potential hydrogen storage materials. There are several groups both in Norway and Switzerland who are already active in this field, and both the number and size of the groups are rapidly increasing. In addition, there is a great deal of interest in the characterization of potential catalytic materials (e.g. metal-organic-framework structures), as well as zeolite-like substances which can be used for “green” (environmentally benign) chemistry. Some of this work has already appeared in print in 2006 [2] and 2007 [3].

While the image plate has the advantage of a large x-ray sensitive area, the CCD detector on the KM6 diffractometer has a much faster readout cycle (about 5s vs. 70s for a typical image). This implies that the CCD is often more suitable for the collection of time-resolved data. The speed of readout can be effectively exploited for single crystal diffraction experiments, particularly if attention is focused on a limited region of reciprocal space. We present here brief reports on two in-house experiments which have exploited the speed of data collection on BM1A. In one case, a reconstruction in reciprocal space allowed the intensity of a superstructure reflection to be monitored as a function of temperature using the CCD detector. In another experiment, the MAR345 image plate was used for monitoring crystal lattice parameters during a temperature ramp. In both cases, the key information could only be extracted from the temperature dependence of the investigated parameters, and not from individual measurements at a few temperatures. The collection of many hundreds of data sets in this fashion is only possible at a synchrotron facility equipped with area detectors.

Superstructure reflections in NdBaCo2O5.5 as seen from a fast experiment with the CCD detector

Interest to rare earth cobaltites is motivated by a complex interplay of spin and orbital degrees of freedom and conjugated effects in structural and magnetic properties. In $RBaCo_2O_{5+\delta}$ (R= rare earth element, $\delta \approx 0.5$) cobalt ions are coordinated by oxygen forming pyramids and octahedra. Depending on ligand field, Co^{3+} ions can be found in low spin state (LS, S= 0, t_{2g}^6, e_g^0), intermediate spin state (IS, S= 1, t_{2g}^5, e_g^1) or high spin state (HS, S= 2, t_{2g}^4, e_g^2). Providing that the energy difference between these states is small, ~k_BT, different electronic degeneracy via an entropy factor leads to a temperature-induced conversion of spin state. Corresponding orbital, spin state, and magnetic structures can be traced by monitoring superstructure reflections in a diffraction experiment. For structural transitions linked to a change of spin state and orbital ordering, superstructures appear due to small displacements of oxygen ions. For both neutron and X-ray diffraction, those diffraction intensities are few orders of magnitude weaker than the main Bragg reflections. However, those weak reflections manifest a change of symmetry that is vital for the understanding of magnetic and spectroscopic properties.

The temperature dependence of selected reflections was monitored with broad phi-scans repeatedly collected during cooling/heating process. The Onyx CCD detector mounted on the KM6 multi-axis diffractometer was used for data collection. The width of the scan was selected to assure that reflection of interest does not leave the scanned zone due to the temperature variation of orientation matrix. The exposure time per image was 10 seconds and the intensity of the superstructure reflections was extracted with help of CrysAlis software supplied by Oxford Diffraction.

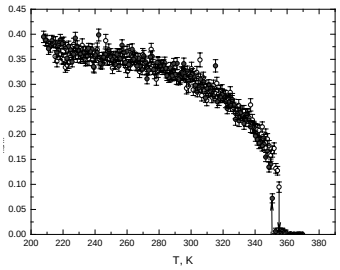

Fig. 1. Intensity of the $\bar{1}18$ reflection as a function of temperature on heating (open symbols) and cooling (grey symbols) modes.

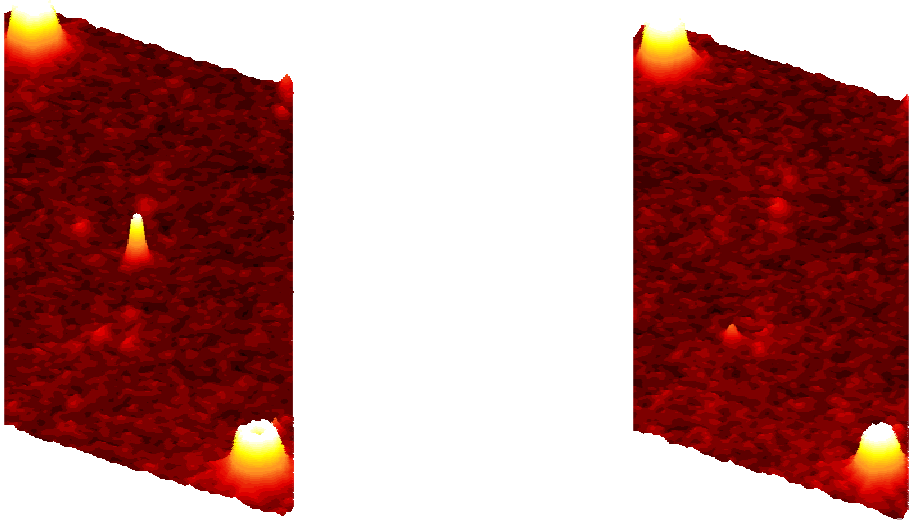

Fig 2. Part of the experimental CCD images below (left) and above (right) the phase transition.

Temperature-dependent investigation of the lattice constants of metallo-organic complex

$Cu_4Cl_6O{\cdot}4L$ compounds contain isolated, oxygen-centered Cu^{2+} tetrahedra, surrounded by chlorine atoms and various organic ligands L. In view of puzzling magnetic properties of these systems, we have studied at various temperatures a system where L is diallylcyanamide (DACA). Powder diffraction data were collected using MAR345 image plate detector. An 80-378 K temperature range was covered with a 1.7 K step in less than 8 hours. The data series were automatically integrated, scaled and fed into the Fullprof software package for sequential refinement using a locally developed program code. As a result, profile and structural parameters can be easily plotted as a function of temperature. Variation of the cell parameters for the tetragonal $Cu_4Cl_6O{\cdot}4DACA$ reveals a crossover-like transition centred at 282.5 K.

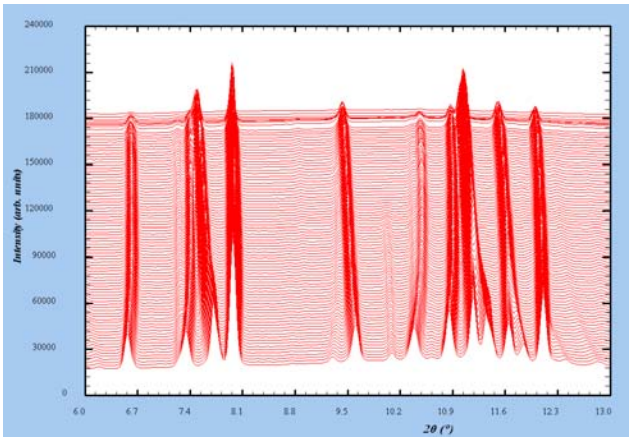

Fig. 3. Powder diffraction data collected upon heating from 273K to 378K

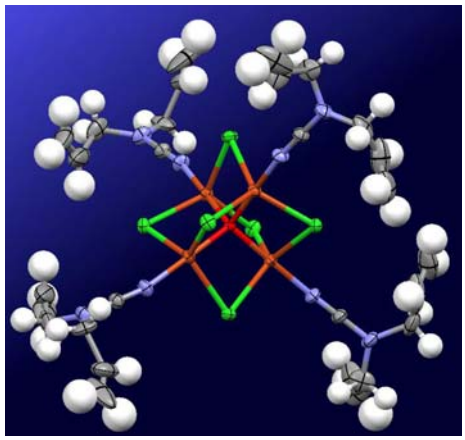

Fig. 4 Disorder in $Cu_4Cl_6O{\cdot}4DACA$ as seen on a single crystal at 293K

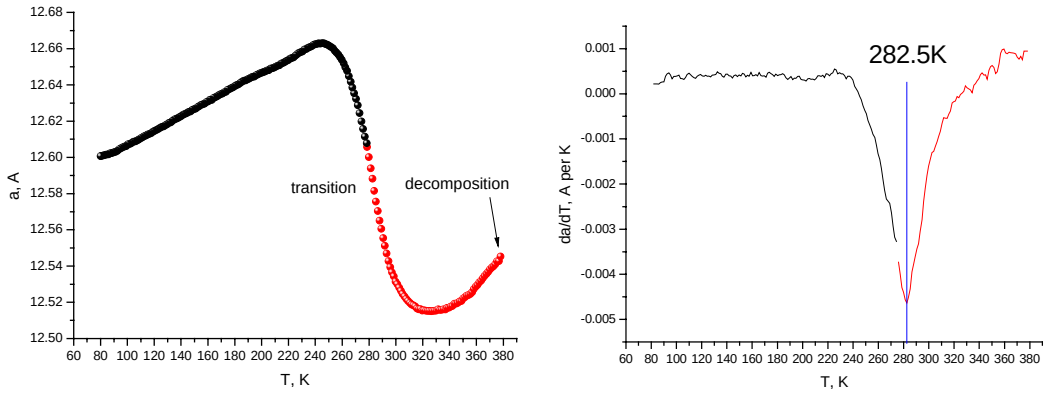

Fig. 5. Temperature dependence of the cell parameter *a* (left) and its first derivative (right)

Cu…Cu and Cu-Cl distances increase only slightly between 80 K and the temperature of decomposition. This suggests that the transition is not related to temperature variations in the Cu_4Cl_6O core, but rather to an order/disorder or reorientation of the flexible parts of the organic molecule. This is supported by a comparison of single-crystal structures determined at SNBL at 80 K and 293 K. A diffraction study of a single crystal at a temperature well above the transition, e.g. at ~350 K, will provide a definitive answer about a mechanism of the transition.

Planned developments at BM1A

Infrastructure

The upgrade of the beamline instrumentation and vacuum control system is part of the overall refurbishment of SNBL. We are now in the process of replacing most of the cables and much of the other infrastructure and controls hardware. It is our goal to complete this refurbishment by the end of 2007.

Beamline optics and diffractometer instrumentation

During several years of operation, we have identified a number of new components and various mechanical modifications which would improve the performance of the KM6 diffractometer. Some upgrades are essential if we are to be able to carry out some new experiments (such as thin film measurements). Most of the improvements can be done on our own timescale, while some others require intervention by the manufacturer. It is also our goal to be able to extend the useful spectral range of BM1A up to 25 keV and beyond, including the possibility of obtaining an optimal focal spot at these energies. Achieving these targets will require investment in hardware and controls for the beamline optics.

Diffractometer software

The software package for diffractometer control from Oxford Diffraction has evolved considerably over the last few years. Now we wish to fix specifications and order a software upgrade from Oxford Diffraction which will be specifically aimed at improvements for the KM6 diffractometer at SNBL. The timescale will be determined by the effort required and the resources available, but we would aim for delivery and testing of the new software by end 2007.

New experimental opportunities

We are in the process of fixing specifications and design parameters for a high gas pressure rig. This apparatus should enable users to reach a combination

of 700bar gas pressure and 500C temperature for their samples. This type of apparatus will open up many new scientific opportunities in the fields of materials science, hydrogen storage, catalysis and many other areas of research. A workshop will be held in 2007 to explore these possibilities.

References

[1] Pattison, P., Kundsen, K.D., Cerny, R., Koller, E. *Rapid characterization of complex structural phase transitions using powder diffraction and an area detector* J. Synchrotron Rad., **7**, 251/256, 2000

[2] Llewellyn, Ph.L., Bourrelly, S., Serre, Ch., Filinchuk, Y., Férey, G. *How hydration drastically improves adsorption selectivity for CO2 over CH4 in the Flexible Chromium Terephthalate MIL-53* Angew. Chem. Int., **45**, 46, 7751 - 7754, 2006

[3] Serre, C., Mellot-Draznieks, C., Surblé, S., Audebrand, N., Filinchuk, Y., Férey, G. *Role of solvent-host interactions that lead to very large swelling of hybrid frameworks* Science, **315**, 5820, 1828 - 1831, 2007

BM1B: HIGH RESOLUTION POWDER DIFFRACTOMETER AND EXAFS SPECTROMETER

H. Emerich

Over the past two years, SNB has been operational without any major interruptions or beam-time losses. The tendency towards increasingly complex experiments has been maintained. By now, about two thirds of the experiments performed on SNB require an *in-situ* set-up and/or the combination of several techniques namely powder diffraction, EXAFS and – in some test experiments - Raman spectroscopy.
In the past, experiments of this type have been reserved for expert users only. Due to substantial improvements in reliability and ease of use of the beamline, combined experiments have become more of a routine these days.
On this basis, we believe that we are now in a position where we can add a Raman spectrometer to our beamline without disrupting the present performance.

Technical and experimental developements:

After the necessary preparational changes during the 2003/2004 period, the past two years have been devoted to two major developments:

A. Conception, construction and implemention of a new double crystal monochromator.
B. Assessment of a novel experimental approach in combining the (quasi-) simultaneous use of powder diffraction, EXAFS and Raman.

A. New Monochromator:

The new monochromator is now working for almost a year and user feedback has been very positive.

The device has been designed around the ever more stringent needs of our EXAFS user community. To give an example: we observed a trend within our catalysis user community to incorporate several metals in the same catalyst in order to fine-tune the active site properties. By doing so, one can obtain better chemical activity, stability and selectivity. The practical consequence for such an in-situ experiment is the need to perform rapid moves between distant absorption edges and/or the possibility to quickly swap between a Si-111 or a Si-311 pair of crystals in order to select the appropriate resolution (typically within a timescale of about one minute).
Furthermore: Considering that the available space around the area where the monochromator had to be installed is very limited (at this location A- and B-branch are separated by about 8 cm only), plus the small diameter of the already existing mono-vessel, imposed severe restrictions on the design.
The following picture gives an overall impression of the layont of the monochromator.

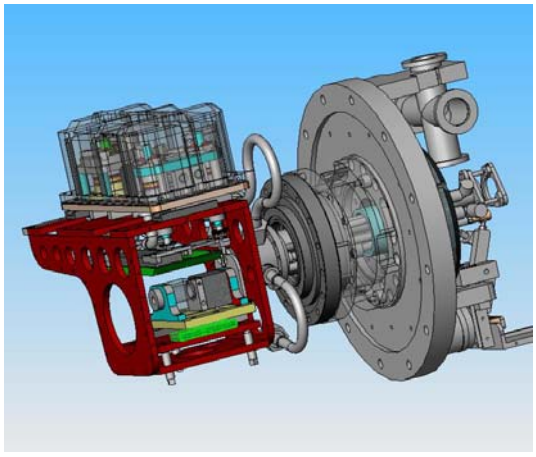

Fig. 1 B-Monochromator

The central features are:
A water-cooled first crystal pair (111/311) is mounted side by side onto a slide (shown in green).

Opposite to it, a titanium cage containing a pair of two 200 mm long Si-111/311 crystals is supported by three actuators (kinematic mount) acting from above. The whole actuatator mechanism sits in an evacuated box (shown as translucent) separated from the vessel vacuum and also mounted on a pair of slides. The actuator motion is transmitted from inside the box via bellows (12mm stroke). This way all the actuator mechanics can be lubricated without spoiling the vessel vacuum.
A piezo integrated into the third actuator (defining the Bragg angle) allows for an active feedback loop. The box vacuum is connected to the outside via bellows and pumped by the same forepump as the one serving the turbo pump sitting on the vessel (not shown) -thus avoiding pressure differences larger than a few millibars. Everything is held together via an Invar cage (red) allowing for a channel-cut like operation due to the long second pair of crystals. A whip mounted outside the vessel permits to simultaneously offset the top and the bottom crystal pair in order to select either the Si-311 or the Si-111 option.
The full design has been made in-house as well as the construction and testing of all pieces, both mechanical and electronical.
Now, after almost one year of operation, most of the initial problems have been ironed out and we can now operate it very close to our initial specifications. The new mono capabilities are briefly illustrated below.

Figure 2 shows an energy scan over the Silver K-edge. It clearly

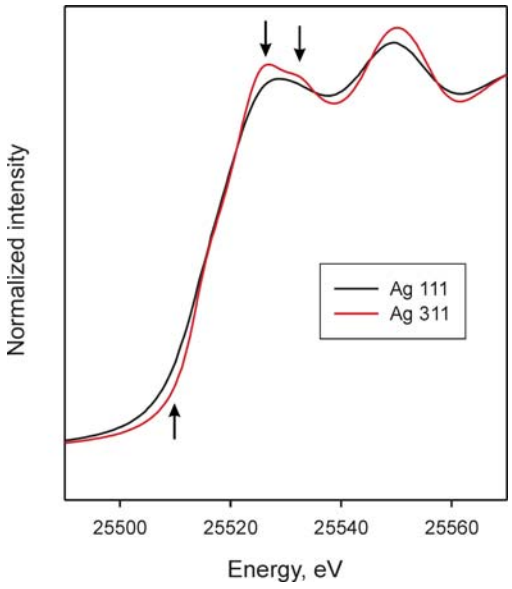

Fig. 2 Ag edge measured with our Si-111 and Si-311 crystals

demonstrates the improvement in resolution due to the Si-311 option.
On the low-energy side, we are presently able to access the Vanadium K-edge. Fig. 3 shows the pre-edge of Vanadium scanned with 0.1 eV steps. Very soon we should also be able to reach the Titanium edge at ~5keV; measurements at this energy range have already been planned. On the high energy side of the energy spectrum, we had no difficulties in reaching the W K-edge at ~70keV.
Figure 4 shows an EXAFS scan over the Tantalum K-edge at 67.42 keV.
As expected, hardly any absorption oscillations can be seen in the raw data (Fig 4). After background substraction and k weighing however

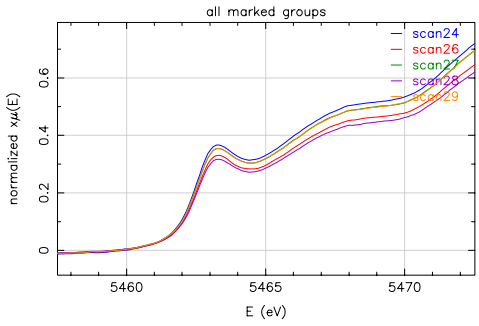

Fig .3. Vanadium pre-edge

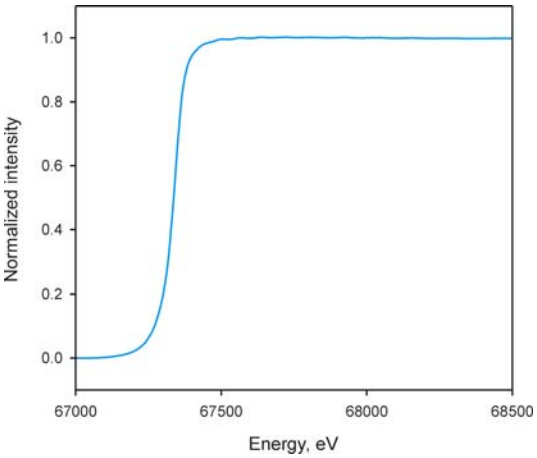

Fig. 4 Ta K-edge

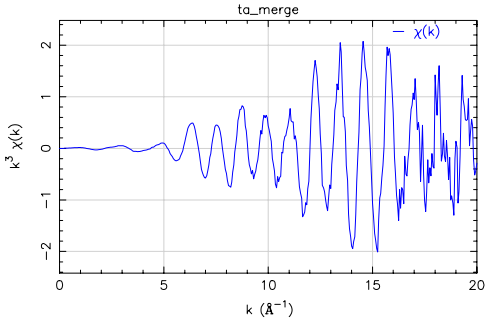

Fig. 5 Ta K-edge Exafs signal, k-weighed.

the EXAFS signal comes out as illustrated in Fig. 5.
Other upgrades made to our EXAFS set-up are: New amplifiers, ion-chambers and gas filling system. Together with the already installed 13 element solid state detector, SNBL's EXAFS set-up is now state of the art. Remaining improvements are the installation of an already delivered set of mirrors, and an improved experimental table.

B. RAMAN Project

Similar to the beamline changes, the Raman project has been driven by the latest and future scientific needs.
X-ray diffraction (XRD) is an important technique to investigate the long range order of atoms and molecules in the solid state.
X-ray Absorption Spectroscopy absorption spectroscopy (XAS) probes the local environement of a given type of atom. In contrast, the Raman technique, gives additional information by its ability to look at individual bonds in the investigated material.

The synergy between these different methodologies has been applied to many scientific studies where Raman and/or XRD/XAS techniques have been performed *ex-situ.* The SNBL staff has initiated a program to combine these complementary techniques by rendering simultaneous *in-situ* Raman / XRD / XAS measurements possible. We believe this approach will open up many new avenues of research and offer vital details in the study of materials and solid state science. Clearly, additional technical developments will have to be made in the future to enable the use of all three techniques under different (non ambient) sample conditions.

To assess the specific needs and possibilities, an extensive testing program has been performed over the past two years.
With a rented Raman spectrometer (Fig. 6), 12 user experiments have been performed on real scientific examples.
This "multi-technique approach" turned out to be particularly beneficial for

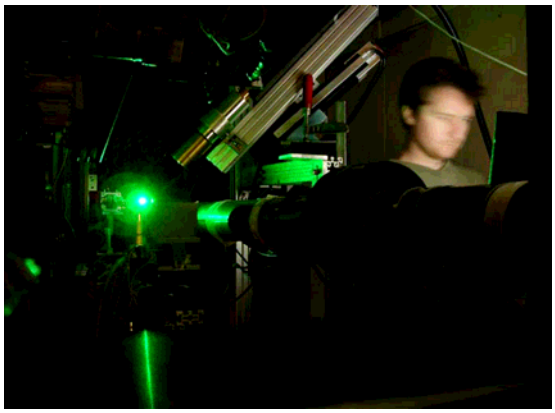

Fig. 6 Alignment of Raman laser.

experiments where samples are changing during the course of the experiment (Excitation by illumination, (de-) hydration, phase transitions, etc). Often transition states can not be reliably reproduced. Therefore all measurements have to be done in-situ and (quasi-) simoultaneously.

The following list gives an idea of the performed experiments, all of them have been performed in-situ:

• High resolution powder experiments between 5K and 1000 K (under UV and laser excitation).
• High temperature 600K Exafs/Raman in reducing and oxidizing environments.
• Xanes/Powder/Raman under hydrothermal synthesis conditions.
• Powder and single crystal crystallization upon melting studied with Raman and single crystal and powder diffraction.

For illustration, two examples are given below:

A) Dehydration of the natural zeolite 'Goosecreekite':
Changes in framework and water vibrations have been investigated by Raman.
Figure 7 shows the changes in the framework vibrations with increasing temperature.

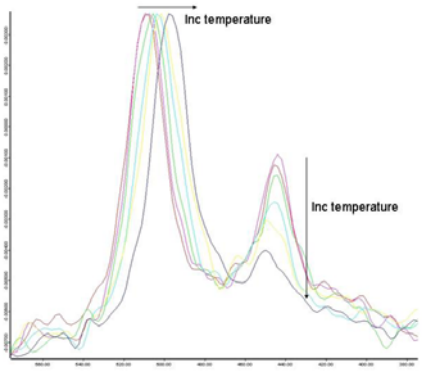

Fig.7 Goosecreekite framework vibrations.

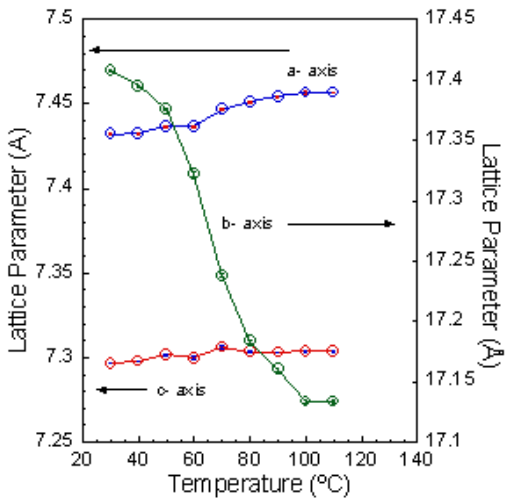

Fig. 8 Goosecreekite Lattice change

Surprisingly the water molecules become less mobile and ice-like upon an increase in temperature (not shown).
Powder diffraction performed at the same time yielded the corresponding lattice parameters shown in Fig. 8.

B) Thermal decomposition of Stearate-hydrotalcite (ST-HYT).
The rearrangement and decomposition processes induced by thermal treatment on a lamellar stearate-hydrotalcite nanocomposite were analyzed under *in situ* conditions.
XRPD data in Fig. 9 yielded information on the inorganic lamellar part of the material. In particular a phase transition, ascribed to the

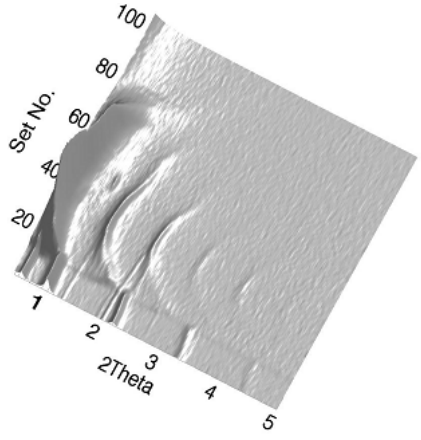

Fig 9. ST-HYT powder data.

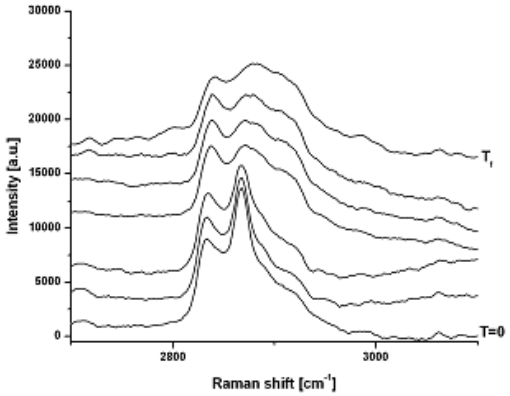

Fig. 10 ST-HYT Raman data

swelling of the layers, can be observed at 368 K. The XRPD pattern does not allow to extract information about the organic molecules.Raman spectroscopy however allows to probe the vibrational modes of the C-H groups (2800-3000 cm-1 range).
In particular, it gives information on the stearate changes during the thermal treatment. The vibrational bands of the C-H stretching become very wide above 368 K, indicating a transition to a liquid-like phase, stable above the stearate melting point, with a change of the conformational freedom of the molecular units, still encapsulated in the lamellar hydrotalcite host.

The success of combined Raman/ XRPD/EXAFS experiments has encouraged us to develop these technique further on SNBL. As things stand at the moment big parts of the funding for a research grade Raman spectrometer are secured and we has been confident that we will be able to integrate a fully working system in a very near future.

Future developements:

The implementation (on a software and hardware level) of a set-up allowing for fully simoultaneous Raman / XRPD / EXAFS measurements will be at the heart of our activities in the mid-term future.
We are also planning a new gas mixing system. Besides the option to deliver changing gases/mixtures to the sample, it should also include other features such as gas pre-heating, and saturating of inert and dangerous supply gases, coupled to a mass-spectrometer at the outlet in order to measure the reaction products.

To summarize: We expect that the combination of the improvements which have already been achieved, together with the changes described above, will allow SNB to be turned into a unique instrument

SNBL - FACTS AND FIGURES

BUDGET (in CHF)

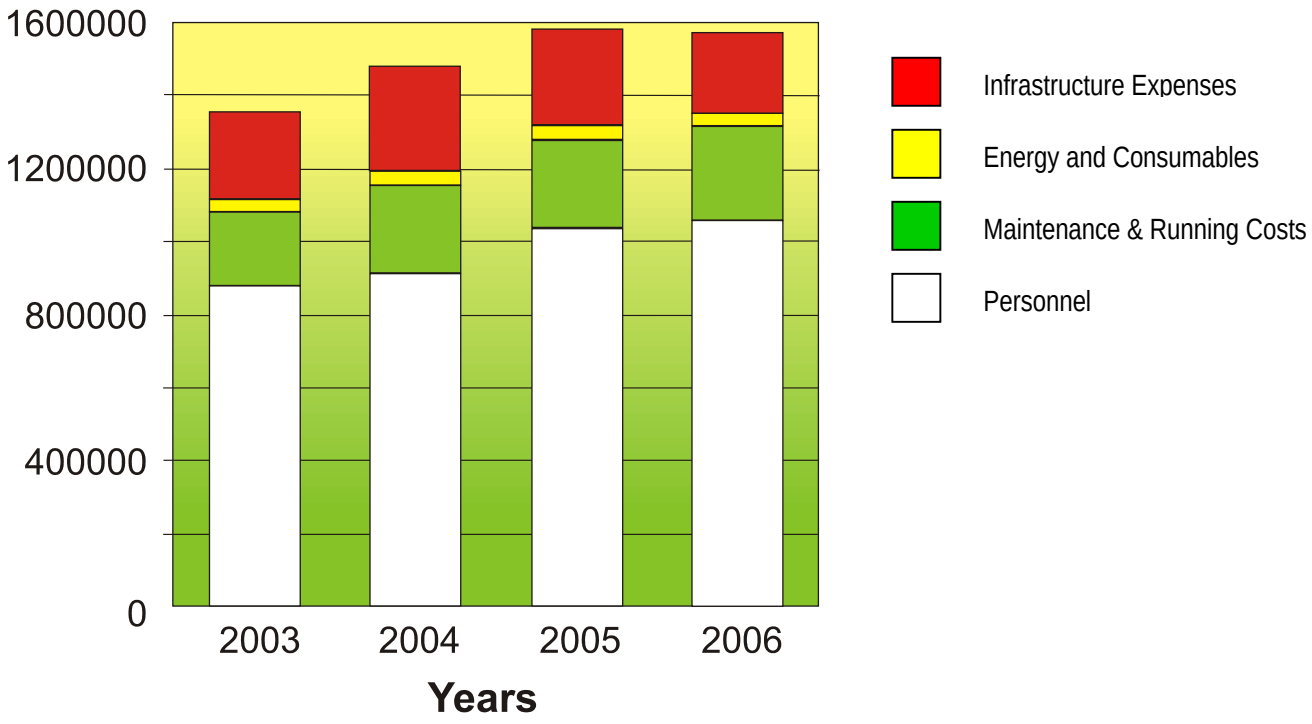

BUDGET in CHF	2003	2004	2005	2006
Personnel	879,000.00	913,000.00	1,037,000.00	1,064,000.00
Maintenance and Running Costs	200,000.00	240,000.00	240,000.00	257,000.00
Energy and Consumables	35,000.00	35,000.00	35,000.00	38,000.00
Infrastructure Expenses	238,000.00	288,000.00	275,000.00	217,000.00
TOTAL	**1,352,000.00**	**1,476,000.00**	**1,588,000.00**	**1,576,000.00**

INCOME (in CHF)

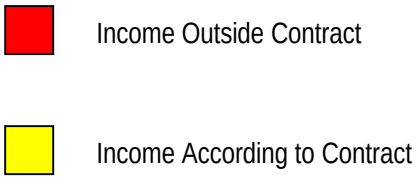

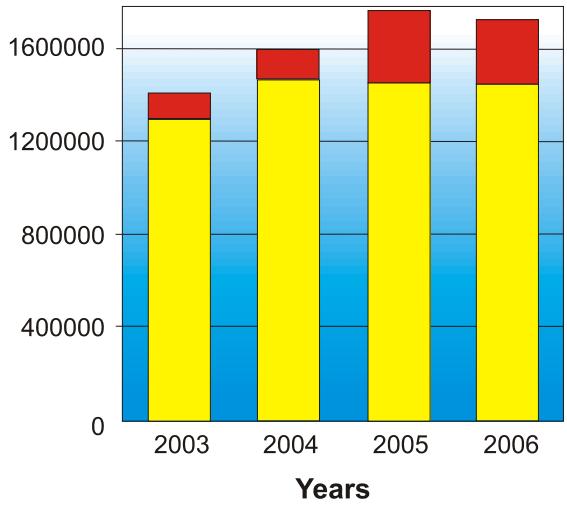

INCOME in CHF	2003	2004	2005	2006
Income According to Contract	1,293,720.00	1,475,000.00	1,450,000.00	1,450,000.00
Income Outside Contract	114,948.00	123,379.00	316,475.00	271,590.00
TOTAL	**1,408,668.00**	**1,598,379.00**	**1,766,475.00**	**1,721,590.00**

EXPENDITURE (in CHF)

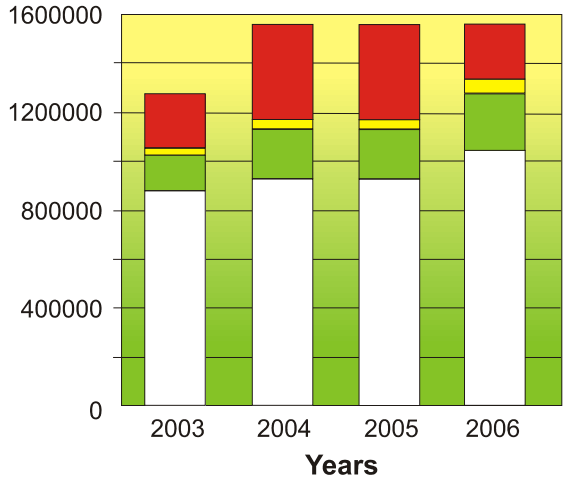

EXPENDITURE in CHF	2003	2004	2005	2006
Personnel	875,000.00	930,000.00	949,000.00	1,056,000.00
Maintenance and Running Costs	154,000.00	198,000.00	218,000.00	239,000.00
Energy and Consumables	29,000.00	45,000.00	45,000.00	61,000.00
Infrastructure Expenses	224,000.00	389,000.00	269,000.00	219,000.00
TOTAL	**1,282,000.00**	**1,562,000.00**	**1,481,000.00**	**1,575,000.00**

PUBLICATIONS

Publication Rate since start-up of SNBL

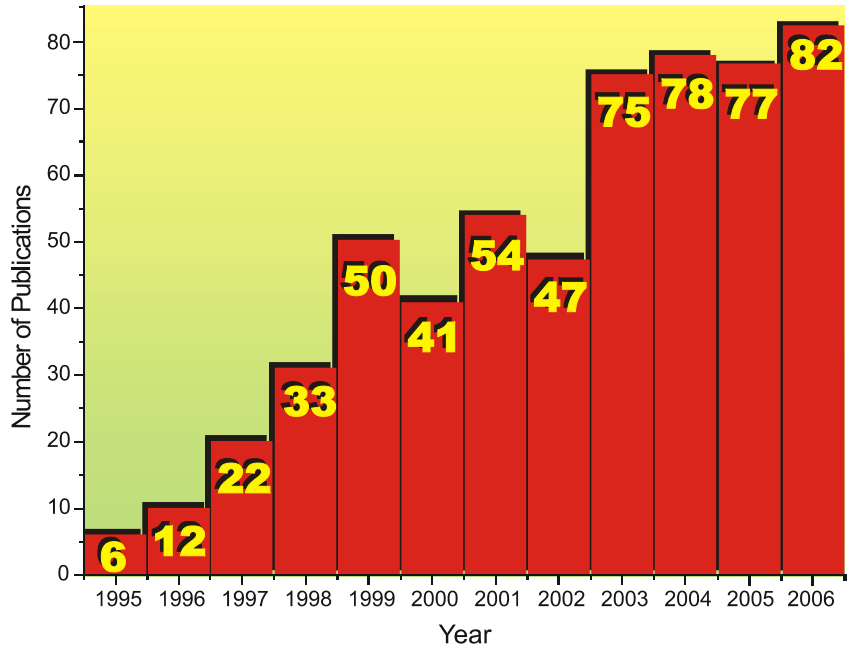

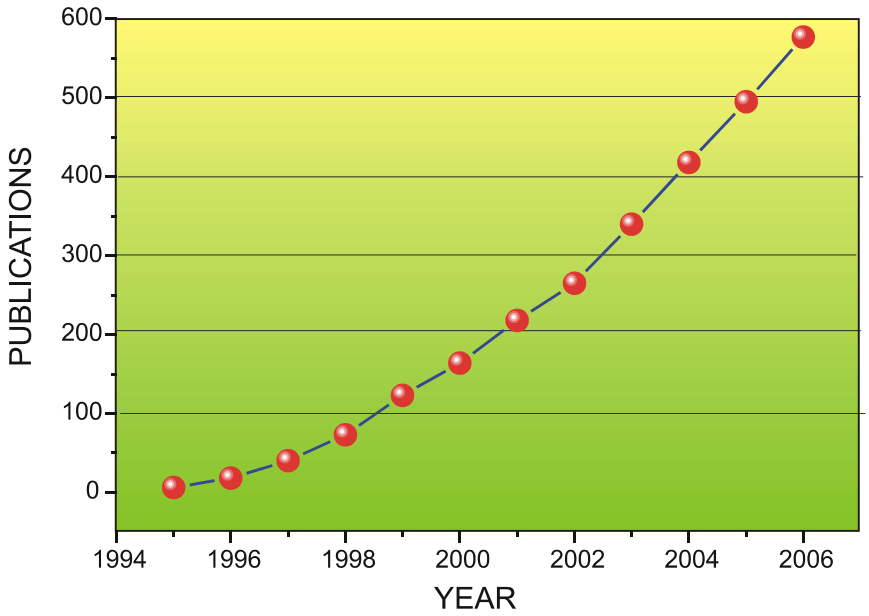

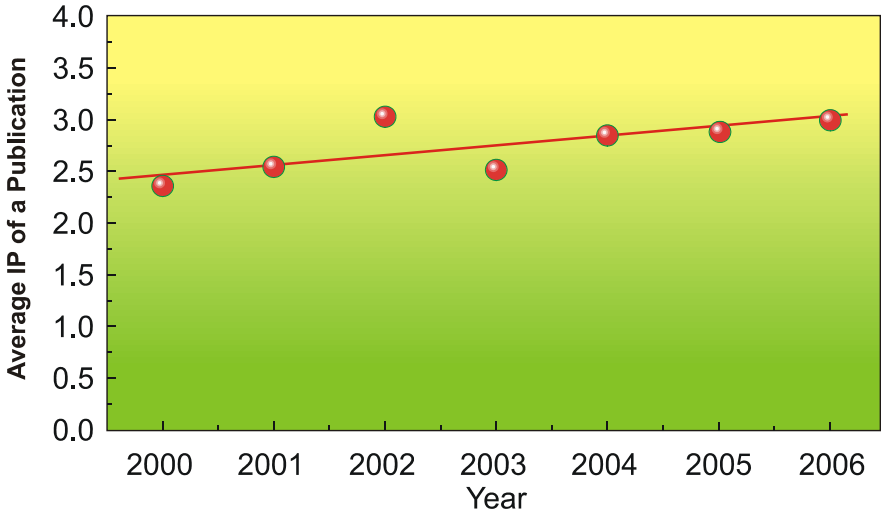

Impact factor of the "average journal" paper produced by the SNBL Users. Straight line is the best least-square fit.

List of Publications

2005

1. Albertsen, J.Z., Grong, Ø., Mathiesen, R.H., Schmid, B. *Metallurgical investigation of metal dusting corrosion in plant-exposed nickel-based alloy 602CA* Corrosion Eng. Science & Technology, 40, 3, 239-243, 2005
2. Beale, A. M., Sankar, G., Nicholson, D. G., VanBeek, W. *In situ study of the crystallisation of nanosized zinc and cobalt aluminate spinel catalysts from ionexchanged zeolite precursors* Physica Scripta, T115, 678-680, 2005
3. Blanchard, D., Brinks, H.W., Hauback, B.C., Norby, P., Muller, J. *Isothermal decomposition of $LiAlD_4$ with and without additives* J. Alloys and Compounds, 404-406, 743-747, 2005
4. Boldyreva, E., Ivashevskaya, S., Sowa, H., Ahsbahs, H., Weber, H.-P. *Effect of hydrostatic pressure on the γ - polymorph of glycine. 1. A polymorphic transition into a new δ-form* Z. Kristallogr., 220, 50-57, 2005
5. Boldyreva, E., Kolesnik, E., Drebushchak, T., Ahsbahs, H., Beukes, J. A., Weber, H.-P. *A comparative study of the anisotropy of lattice strain induced in the crystals of L-serine by cooling down to 100 K or by increasing pressure up to 4.4 GPa* Z. Kristallogr., 220, 58-65, 2005
6. Bricogne, G., Capelli, S.C., Evans, G., Mitschler, A., Pattison, P., Roversi, P., Schiltz, M. *X-ray absorption, refraction and resonant scattering tensors in selenated protein crystals: implications for data collection strategies in macromolecular crystallography* J. Appl. Cryst., 38, 168-182, 2005
7. Brinks, H.W., Fossdal, A., Fonneløp, J.E., Hauback, B.C. *Crystal structure and stability of $LiAlD_4$ with TiF_3 additive* J. Alloys and Compounds, 397, 1-2, 291-295, 2005
8. Brinks, H.W., Hauback, B.C., Jensen, C.M., Zidanc, R. *Synthesis and crystal structure of Na_2LiAlD_6* J. Alloys and Compounds, 392, 1-2 , 27-30, 2005
9. Brinks, H.W., Hauback, B.C., Srinivasan, S. S., Jensen, C. M. *Synchrotron X-ray studies of $Al_{1-y}Ti_y$ formation and Re-hydriding inhibition in Ti-enhanced $NaAlH_4$* J. Phys. Chem. B, 109, 33, 15780 -15785, 2005
10. Bürgi, H. B., Hauser, J. *Supramolecular architecture in a disordered perhydrotriphenylene inclusion compound from diffuse X-ray diffraction data* Crystal Growth & Design, 5, 6, 2073 -2083, 2005
11. Bus, E., Miller, J. T., Van Bokhoven, J. A. *Hydrogen chemisorption on Al_2O_3-supported gold catalysts* J. Phys. Chem. B, 109, 30, 14581 -14587, 2005

12. Cerný, R., Favre-Nicolin, V. *FOX: A friendly tool to solve nonmolecular structures from powder diffraction* Powder Diffraction, 20, 4, 359-365, 2005
13. Cruciani, G., Matteucci, F., Dondi, M., Baldi, G., Barzanti, A. *Structural variations of Cr-doped (Y,REE)AlO_3 perovskites* Z. Kristallographie, 220, 11, 930-937, 2005
14. Dubarry, M., Gaubicher, J., Guyomard, D., Durupthy, O., Steunou, N., Livage, J., Dupré, N., Grey, C.P. *Sol gel synthesis of $Li_{1+\alpha}V_3O_8$. 1. From pecursors to xerogel* Chem. Mater., 17, 9, 2276 - 2283, 2005
15. Dubrovinskaia, N., Dubrovinsky, L., Kantor, I., Crichton, W. A., Dmitriev, V., Prakapenka, V., Shen, G., Vitos, L.,Ahuja, R. , Johansson, B., Abrikosov, I. A. *Beating the miscibility barrier between Iron group elements and magnesium by high-pressure alloying* Phys. Rev. Lett., 95, 245502, 2005
16. Filinchuk, Y. E., Yvon, K. *Boron-Induced hydrogen localization in the novel metal hydride $LaNi_3BH_x$ (x = 2.5-3.0)* Inorg. Chem., 44, 12, 4398 -4406, 2005
17. Filinchuk, Y. E., Yvon, K. *Deuterium-induced copper pairing in $Zr_2CuD_{\sim 5}$* Inorg. Chem., 44, 23, 8191 - 8193, 2005
18. Fossdal, A., Brinks, H.W., Fichtner, M., Hauback, B.C. *Determination of the crystal structure of $Mg(AlH_4)_2$ by combined x-ray and neutron diffraction* J. Alloys and Compounds, 387, 1-2, 47-51, 2005
19. Fossdal, A., Brinks, H.W., Fichtner, M., Hauback, B.C. *Thermal decomposition of $Mg(AlH_4)_2$ studied by in situ synchrotron X-ray diffraction* J.Alloys & Compounds, 404-406, 752-756, 2005
20. Fossdal, A., Brinks, H.W., Fonneløp, J.E., Hauback, B.C. *Pressure–composition isotherms and thermodynamic properties of TiF_3-enhanced Na_2LiAlH_6* J. Alloys and Compounds, 397, 1-2 , 135-139, 2005
21. Grunwaldt, J.-D., Kiener, C., Schüth, F., Baiker, A. *X-ray absorption spectroscopy on CuZnO catalysts selected by high throughput experimentation techniques* Physica Scripta, T115, 819-821, 2005
22. Grzechnik, A., Dmitriev, V., Weber H.-P. *Dilithium zirconium hexafluoride Li_2ZrF_6 at high pressures: A new monoclinic phase* J. Phys.& Chem. of Solids, 66, 10, 1769-1774, 2005
23. Grzechnik, A., Friese, K., Dmitriev, V., Weber H.-P., Gesland J.-Y., Crichton, W. *Pressure-induced tricritical phase transition from the scheelite structure to the fergusonite structure in $LiLuF_4$* J.Phys.: Condens. Matter, 17, 763-770, 2005
24. Iosub, V., Joubert, J.-M., Latroche, M., Cerný, R., Percheron-Guégan, A. *Hydrogen cycling induced diffraction peak broadening in C14 and C15 Laves phases* J. Solid State Chem., 178, 6, 1799-1806 2005
25. Johnsen, L., Dalhus, B., Leiros, I., Nissen-Meyer, J. *1.6 Å crystal structure of EntA-Im: A bacterial immunity protein conferring immunity to the antimicrobial activity of the pediocin-like bacteriocin enterocin A* J. Biol. Chem., 280, 19, 19045-19050, 2005
26. Jordá, J.L., Prokic, S., McCusker, L. B., Baerlocher, C., Chun Feng Xue, Dong, J. *Synthesis and structure analysis of the potassium calcium silicate CAS-1. Application of a texture approach to structure solution using data collected in transmission mode* Comptes Rendus Chimie, 8, 3-4, 331-339, 2005
27. Joubert, J.-M., Cerny, R., Latroche, M., Percheron-Gueguan, A., Yvon, K. *Compressibility and thermal expansion of $LaNi_5$ and its substitutional derivatives ($LaNi_{5-x}M_x$; M=Mn, Al,Co)* Intermetallics, 13, 227-231, 2005
28. Kallen, J., Sedrani, R., Zenke, G., Wagner, J. *Structure of human cyclophilin A in complex with the novel immunosuppressant sanglifehrin A at 1.6 Å resolution* J. Biol. Chemistry, 280, 23, 21965-21971, 2005
29. Karau, F. W., Schnick, W. *High-pressure synthesis and X-ray powder structure determination of the nitridophosphate BaP_2N_4* J. Solid State Chemistry, 178, 1, 135-141, 2005
30. Kobas, M., Weber, Th., Steurer, W. *Structural disorder in the decagonal Al–Co–Ni. I. Patterson analysis of diffuse x-ray scattering data* Phys. Rev., B 71, 224205, 2005
31. Kohlmann, H., Renaudin, G., Yvon, K., Wannek, C., Harbrecht, B. *Hydrogen-induced atomic rearrangement in $MgPd_3$* J. Solid State Chemistry, 178, 4, 1292-1300, 2005

32. Kohlmann, H., Yvon, K., Wang, Y. *Synthesis, crystal structure and magnetism of the mixed metal hydrides $Eu_{1-x}Sr_xMg_2H_6$ (0 <= x <= 0.6)* _J. Alloys and Compounds, 393, 1-2, 11-15, 2005
33. Kolberg, M., Logan, D.T., Bleifuss, G., Pötsch, S., Sjöberg, B.-M. Gräslund, A., and al. *A new tyrosyl radical on Phe^{208} as ligand to the diiron center in escherichia coli ribonucleotide reductase, mutant R2-Y122H* J. Biol. Chemistry, 280, 12, 11233-11246, 2005
34. Kuelpmann, A., Osman, M.A., Kocher, L., Suter, U.W. *Influence of platelet aspect ratio and orientation on the storage and loss moduli of HDPE-mica composites* Polymer, 46, 2, 523-530, 2005
35. Maehlen, J.P., Stange, M., Yartys, V.A., Delaplane, R.G. *Hydrogen assisted order–disorder transformations in Cu–Sn sublattices of the (La,Ce)CuSn–D_2 systems* J. Alloys and Compounds, 404-406 , 112-117, 2005
36. Martucci, A., Alberti, A., Cruciani, G., Frache, A., Marchese, L., Pastore, H.O. *Temperature-induced transformations in CoAPO-34 molecular sieve: a combined in situ X-ray diffraction and FTIR study* J. Phys. Chem. B, 109, 28, 13483 -13492, 2005
37. Mathisen, K., Nicholson, D. G., Fitch, A. N., Stockenhuber, M. *Selective catalytic reduction of NOx over microporous CuAPO-5: structural characterisation by XAS and XRD* J. Mater. Chem., 15, 204-217, 2005
38. Mathisen, K., Nicholson, D. G., Stockenhuber, M. *The influence of silicon on the catalytic properties of CuSAPO-5 towards the selective reduction of NO_x in the presence of propene* Microp. & Mesop. Materials, 84, 1-3 , 261-274, 2005
39. Miletich, R., Hejny, C., Krauss, G., Ullrich, A. *Diffraction techniques: Shedding light on structural changes at extreme conditions in Mineral Behaviour at Extereme Conditions* EMU Notes in Mineralogy (Eotovos Univ. Press, Budapest), 7, 281, 2005
40. Nachtegaal, M., Scheidegger, A. M., Dähn, R., Chateigner, D., Furrer, G. *Immobilization of Ni by Al-modified montmorillonite: A novel uptake mechanism* Geochimica et Cosmochimica Acta, 69, 17, 4211-4225, 2005
41. Nazaraly, M., Wallez, G., Chanéac, C., Tronc, E., Ribot, F., Quarton, M., Jolivet, J. -P. *The first structure of a cerium(IV) phosphate: ab initio rietveld analysis of $Ce^{IV}(PO_4)(HPO_4)_{0.5}(H_2O)_{0.5}$* Angewandte Chemie Int. Ed., 44, 35, 5691 - 5694, 2005
42. Nicosia, D., Prins, R. *The effect of glycol on phosphate-doped $CoMo/Al_2O_3$ hydrotreating catalysts* J. Catalysis, 229, 2, 424-438, 2005
43. Oudenhuijzen, M. K., Van Bokhoven, J. A., Miller, J. T., Ramaker, D. E., Koningsberger, D. C. *Three-site model for hydrogen adsorption on supported platinum particles: influence of support Ionicity and particle size on the hydrogen coverage* J. Am. Chem. Soc., 127, 5, 1530 -1540, 2005
44. Paillaud, J.-L., Marichal, C., Roux, M., Baerlocher, Ch., Chézeau, J. M. *Tripling of the Unit Cell Volume of the Non-centrosymmetric AlPO4-SOD after Dehydration: A Structural Study of a Reversible Process* J. Phys. Chem. B, 109, 24, 11893 -11899, 2005
45. Paul-Boncour, V., Guillot, M., André, G., Bourée, F., Wiesingerd, G., Percheron-Guégan, A. *Origin of the first order magnetostructural transition in YFe2D4.2* J. Alloys& Compounds, 404-406, 355-359, 2005
46. Ramin, M., Grunwaldt, J.-D., Baiker, A. *Behavior of homogeneous and immobilized zinc-based catalysts in cycloaddition of CO_2 to propylene oxide* J. Catalysis, 234, 2, 256-267, 2005
47. Renaud, J., Bischoff, S. F., Buhl, T., Floersheim, P., Fournier, B., Geiser, M., Halleux, C. and al. *Selective estrogen receptor modulators with conformationally restricted side chains. Synthesis and structure-activity relationship of Er-alpha-selective tetrahydroisoquinoline ligands* J. Med. Chem., 48, 364-379, 2005
48. Rohr, M., Grunwaldt, J.-D., Baiker, A. *A simple route to highly active ruthenium catalysts for formylation reactions with hydrogen and carbon dioxide* J. Mol. Catalysis A: Chemical, 226, 2, 253-257,2005
49. Rohr, M., Grunwaldt, J.-D., Baiker, A. *Formylation with supercritical carbon dioxide over Ru/Al_2O_3 modified by phosphines: heterogeneous or*

homogeneous catalysis? J. Catalysis, 229, 144-153, 2005

50. Rohr, M., Günther, M., Jutz, F., Grunwaldt, J.-D., Emerich, H., Van Beek, W., Baiker, A. *Evaluation of strategies for the immobilization of bidentate ruthenium–phosphine complexes used for the reductive amination of carbon dioxide* Applied Catalysis A: General, 296, 2 , 238-250, 2005
51. Rønning, M., Huber, F., Meland, H., Venvik, H., De Chen, Holmen, A. *Relating catalyst structure and composition to the water–gas shift activity of Cu–Zn-based mixed-oxide catalysts* Catalysis Today, 100, 3-4, 249-254, 2005
52. Rumyantseva, M.N., Kovalenko, V.V., Gaskov, A.M., Pagnier, T., Machon, D., Arbiol, J., Morante, J.R. Nanocomposites SnO2/Fe2O3: Wet chemical synthesis and nanostructure characterization Sensors and Actuators B: Chem., 109, 1, 64-74, 2005
53. Sato, M., Denys, R.V., Riabov, A.B., Yartys, V.A. Influence of Al- and Cu-doping on the thermodynamic properties of the LaNiIn–H system J. Alloys & Compounds, 400,1-2, 184-187, 2005
54. Sato, M., Stange, M., Maehlen, J. P., Yartys, V. A. *Crystal structure of $LaNi_5Sn$* J. Alloys and Compounds, 397, 1-2, 165-168, 2005
55. Simoncic, P., Armbruster, Th. *Cationic methylene blue incorporated into zeolite mordenite-Na: a single crystal X-ray study* Microp. & Mesop. Materials, 81, 1-3, 87-95, 2005
56. Snell, E.H., Helliwell, J.R. *Macromolecular crystallization in microgravity* Rep. Prog. Phys. 68, 799-853, 2005
57. Sørby, M.H., Fjellvåg, H., Hauback, B.C. *In situ powder synchrotron and neutron diffraction study of Zr_2Ni deuterides* J. Alloys and Compounds, 394, 1-2 , 107-115, 2005
58. Srinivasan, S.S., Jensen, C. M. *Dehydrogenation kinetics and long term cycling behavior of Titanium doped $NaAlH_4$* Mater. Res. Soc. Symp. Proc., 837, 2005
59. Stange, M., Maehlen, J.P., Yartys, V.A., Norby, P., Van Beek, W., Emerich, H. *In situ SR-XRD studies of hydrogen absorption–desorption in $LaNi_{4.7}Sn_{0.3}$* J. Alloys and Compounds, 404-406, 604-608, 2005
60. Stange, M., Paul-Boncour, V., Latroche, M., Percheron-Guégan, A., Isnard, O., Yartys, V.A. *Ce-valence state and hydrogen-induced volume effects in Ce-based intermetallic compounds and their hydrides* J. Alloys and Compounds, 404-406, 144-149, 2005
61. Staub, U., Shi, M., Schulze-Briese, C., Patterson, B. D., Fauth, F., Dooryhee, E. & al. *Temperature dependence of the crystal structure and charge ordering in Yb_4As_3* Phys. Rev. B, 71, 075115, 2005
62. Steurer, W. *Structural phase transitions from and to the quasicrystalline state* Acta Cryst., A61, 28-38, 2005
63. Swamy, V., Dubrovinsky, L., Dubrovinskaia, N., Langenhorst, F., Simionovici, A., Drakopoulos, M., Dmitriev, V., Weber, H. -P. *Size effects on the structure and phase transition behavior of baddeleyite TiO_2* Solid State Comm., 134, 8, 541-546, 2005
64. Szytula, A., Isnard, O., Yartys, V.A., Riabov, A.B. *Crystal and magnetic structure of $HoNiSnD_{0.67}$* J. Alloys & Compounds, 404-406, 200-203, 2005
65. Talyzin, A. V., Langenhorst, F. , Dubrovinskaia, N. , Dub, S., Dubrovinsky, L. S. *Structural characterization of the hard fullerite phase obtained at 13 GPa and 830 K* Phys. Rev. B 71, 115424, 2005
66. Thorkildsen, G. , Larsen, H. B., Weckert, E., Mo, F., Mathiesen, R. H. *Three-beam resonant X-ray diffraction in germanium - Laue transmission cases* Acta Cryst., A61, 460-470, 2005
67. Törnroos, K.W., Chernyshov, D., Hostettler, M., Bürgi, H.-B. *Co-crystallized cis and trans isomers of dichlorobis(2-picolylamine)iron(II)* Acta Cryst., C61, 450-452, 2005
68. Tuel, A., Jorda, J.-L., Gramlich, V., Baerlocher, Ch. *Synthesis and characterization of two aluminophosphates templated by N-methyl-1,3-diaminopropane* J. of Solid State Chem., 178, 782-791, 2005
69. Voegelin, A., Pfister, S., Scheinost, A. C., Marcus, M. A., Kretzschmar, R. *Changes in zinc speciation in field soil after contamination with zinc oxide* Environ. Sci. Technol., 39, 17, 6616 -6623, 2005

70. Vrålstad, T., Øye, G., Rønning, M., Glomm, W. R., Stöcker, M., Sjöblom, J. *Interfacial chemistry of cobalt(II) during sol–gel synthesis of cobalt-containing mesoporous materials* Microp. & Mesop. Mat., 80, 291-300, 2005
71. Vukojevic,S., Trapp, O., Grunwaldt, J.-D., Kiener, Ch., Schüth, F. *Quasi-Homogeneous methanol synthesis over highly active copper nanoparticles* Angewante Chem. Int. Ed., 44, 48 , 7978 - 7981, 2005
72. Wattanasin, S., Kallen, J., Myers, S., Guo, Q., Sabio, M., Ehrhardt, C., Albert, R., Hommel, U., Weckbecker, G., Welzenbach, K., Weitz-Schmidt, G. *1,4-Diazepane-2,5-diones as novel inhibitors of LFA-1* Bioorg.& Med. Chem. Letters, 15, 4, 1217-1220, 2005
73. Weiher, N., Bus, E., Gorzolnik, B., Möller, M., Prins, R., Van Bokhoven, J. A. *An in situ and operando X-ray absorption spectroscopy setup for measuring sub-monolayer model and powder catalysts* J. Synchrotron Rad., 12, 675-679, 2005
74. Wiesinger, G ., Paul-Boncour, V ., Filipek, S. M., Reichl, Ch., Marchuk, I.,Percheron-Guégan, A. *Structural and magnetic properties of RFe_2D_x deuterides (R = Zr, Y and x => 3.5) studied by means of neutron diffraction and ^{57}Fe Mössbauer spectroscopy* J. Phys.: Condens. Matter, 17, 893-908, 2005
75. Wijnhoven, J. E.G.J. *Seeded growth of monodisperse gibbsite platelets to adjustable sizes* J. Colloid& Interface Science, 292, 2 , 403-409, 2005
76. Zbinden, K. G., Banner, D. W., Ackermann, J., D'Arcy, A., Kirchhofer, D., Ji, Y.-H., Tschopp, T. B., Wallbaum, S., Weber, L. *Design of selective phenylglycine amide tissue factor/factor VIIa inhibitors* Bioorganic & Medicinal Chem. Letters, 15, 3, 817-822, 2005
77. Zbinden, K. G., Obst-Sander, U., Hilpert, K., Kühne, H., Banner, D. W., Böhm, H.-J., Stahl, M., Ackermann, J., Alig, L., Weber, L., Wessel, H. P., Riederer, M. A., Tschopp, Th. B., Lavé, Th. *Selective and orally bioavailable phenylglycine tissue factor/factor VIIa inhibitors* Bioorganic & Medicinal Chem. Letters,15, 23, 5344-5352, 2005

2006

1. Altermark, B., Smalås, A.O., Willassen, N.P., Helland, R. *The structure of Vibrio cholerae extracellular endonuclease I reveals the presence of a buried chloride ion* Acta Cryst., D62, 1387-1391, 2006
2. Avdoshenko, S., Goryunkov, A., Ioffe, I., Ignat'eva, D., Sidorov, L., Pattison, Ph., Kemnitz, E., Troyanov, S. *Preparation, crystallographic characterization and theoretical study of $C_{70}(CF_3)_{16}$ and $C_{70}(CF_3)_{18}$* Chem. Commun., 2463 - 2465, 2006
3. Birkedal, H., Andersen, A.M.K., Arakcheeva, A., Chapuis, G., Norby, P., Pattison, P. *The room-temperature superstructure of ZrP_2O_7 is orthorhombic: there are no unusual 180° P-O-P Bond Angles* Inorg. Chem., 45, 11, 4346 - 4351, 2006
4. Birkedal Nielsen, R.K., Kongshaug, K.O., Fjellvåg, H. *Syntheses, crystal structures and thermal properties of 3D coordination polymers assembled from 1,4,5,8-naphthalenetetracarboxylic acid* Solid State Sciences, 8, 10, 1237-1242, 2006
5. Birkedal, H., Pattison, P. *Bis[4-(salicylideneamino) phenyl] methane* Acta Cryst. C Crystal Structure Comm., 62, 3, 139-141, 2006
6. Boldyreva, E., Ahsbahs, H., Chernyshev, V., Ivashevskaya, S., Oganov, A. *Effect of hydrostatic pressure on the crystal structure of sodium oxalate: X-ray diffraction study and ab initio simulations* Z. Kristallogr., 221, 3, 186-197, 2006
7. Boldyreva, E., Dmitriev, V., Hancock, B. *Effect of pressure up to 5.5 GPa on dry powder samples of chlorpropamide Form-A* International J.Pharmaceutics, 327, 51-57, 2006
8. Boldyreva, E.V., Sowa, H., Seryotkin, Yu.V., Drebushchak, T.N., Ahsbahs, H., Chernyshev, V., Dmitriev, V. *Pressure-induced phase transitions in crystalline L-serine studied by single-crystal and high-resolution powder x-ray diffraction* Chemical Physics Letters, 429, 4-6, 474-478, 2006
9. Bonhoure, I., Baur, I., Wieland, E., Johnson, C. A., Scheidegger, A. M. *Uptake of Se(IV/VI) oxyanions by*

hardened cement paste and cement minerals: An X-ray absorption spectroscopy study Cement and Concrete Research, 36, 1, 91-98, 2006

10. Boulineau, A., Joubert, J.-M., Cerný, R. *Structural characterization of the Ta-rich part of the Ta–Al system* J. Solid State Chem., 179, 11, 3385-3393, 2006
11. Brinks, H.W., Istad-Lem, A., Hauback, B.C. *Mechanochemical synthesis and crystal structure of α'-AlD_3 and α-AlD_3* J. Phys. Chem. B, 110, 51, 25833 -25837, 2006
12. Brinks, H.W., Sulic, M., Jensen, C. M., Hauback, B. C. *TiCl_3-enhanced $NaAlH_4$: impact of excess Al and development of the $Al_{1-y}Ti_y$ phase during cycling* J. Phys. Chem., 110, 6, 2740 -2745, 2006
13. Canton, P., Fichtner, M., Frommen, M., Léon, A. *Synchrotron X-Ray Studies of Ti-Doped $NaAlH_4$* J. Phys. Chem., 110, 7, 3051 -3054, 2006
14. Cerný, R., Renaudin, G., Tokaychuk, Y., Favre-Nicolin, V. *Complex intermetallic compounds in the Mg-Ir system solved by powder diffraction* Z. Kristallog. Suppl., 23, 411-416, 2006
15. Chotard, J.-N., Filinchuk, Y., Revaz, B., Yvon, K. *Isolated $[Ni_2H_7]^{7-}$ and $[Ni_4H_{12}]^{12-}$ Ions in $La_2MgNi_2H_8$* Angew.Chem.Int., 45, 1-4, 2006
16. Christensen, M., Lock, N., Overgaard, J., Iversen, Bo B. *Crystal structures of thermoelectric n- and p-type $Ba_8Ga_{16}Ge_{30}$ studied by single crystal, multitemperature, neutron diffraction, conventional X-ray diffraction and resonant synchrotron X-ray diffraction* J. Am. Chem. Soc., 128, 15657-15665, 2006
17. Dalconi, M. C., Cruciani, G., Alberti, A., Ciambelli, P. *Over-loaded Cu-ZSM-5 upon heating treatment: A time resolved X-ray diffraction study* Microp.& Mesop. Materials, 94, 1-3 , 139-147, 2006
18. Damay, F., Carretero-Genevrier, A., Cousson, A., Van Beek, W., Rodriguez-Carvajal, J., Fillaux, F. *Synchrotron and neutron diffraction study of 4-methylpyridine-N-oxide at low temperature* Acta Cryst. B62, Structural Science, 627-633, 2006
19. Dähn, R., Jullien, M., Scheidegger, A.M., Poinssot, Ch., Baeyens, B., Bradbury, M.H. *Identification of neoformed Ni-phyllosilicates upon Ni uptake in montmorillonite: a transmission electron microscopy and extended X-Ray absorption fine structure study* Clays and Clay Minerals, 54, 2, 209 -- 219, 2006
20. De Armas, H.N., Peeters, O.M., Blaton, N., De Ridder, D. J. A., Schenk, H. *X-ray powder diffraction data and crystal data of polymorphic form 2 of carnidazole* Powder Diffraction, 21, 1, 56-58, 2006
21. De Armas, H.N., Peeters, O.M., Blaton, N., Van den Mooter, G., De Ridder, D.J.A., Schenk, H. *Crystal structure of carnidazole form II from synchrotron X-ray powder diffraction: Structural comparison with form I, the hydrated form and the low energy conformations in vacuo* J. Pharmaceutical Sci., 95,10, 2123 - 2136, 2006
22. Dietzel, P. D. C., Panella, B., Hirscher, M., Blom, R., Fjellvåg, H. *Hydrogen adsorption in a nickel based coordination polymer with open metal sites in the cylindrical cavities of the desolvated framework* Chemical Communications, 959 - 961, 2006
23. Dmitriev, V.P., Dubrovinsky, L., Le Bihan, T., Kuznetsov, A., Weber, H.-P., Poniatovsky, E.G. *Collapsed hexagonal ω phase in a compressed TiZr alloy: Angle-dispersive synchrotron-radiation x-ray diffraction study* Phys. Rev. B, 73, 094114-094120, 2006
24. Dorozhkin, E.I., Ignat'eva, D.V., Tamm, N.B., Vasilyuk, N.V., Goryunkov, A.A., Avdoshenko, S.M., Ioffe, I.N., Sidorov, L.N., Pattison, Ph. at al. *Structure of 1,4,10,19,25,41-C70(CF3)6, isomer with unique arrangement of addends* J. Fluorine Chem., 127, 10, 1344-1348, 2006
25. Dubarry, M., Gaubicher, J., Guyomard, D., Steunou, N., Livage, J., Dupré, N., Grey, C.P. *Synthesis of $Li_{1+\alpha}V_3O_8$ via a Gel Precursor: Part II, from Xerogel to the Anhydrous Material* Chem. Mater., 18, 3, 629 - 636, 2006
26. Filinchuk, Y.E., Sheptyakov, D., Yvon, K. *Directional metal-hydrogen bonding in interstitial hydrides II. Structural study of $HoNi_3D_x$ (x = 0, 1.3, 1.8)* J. Alloys and Compounds, 413, 1-2, 106-113, 2006
27. Filinchuk, Y.E., Yvon, K. *Directional metal–hydrogen bonding in interstitial hydrides III: Structural study of $ErCo_3D_x$*

(0<=x<=4.3) J. Solid State Chemistry, 179, 4, 1041-1052, 2006

28. Fossum, J.O., Méheust, Y., Palmar, K.P.S., Knudsen, K.D., Måloy, K.J., Fonseca, D.M. *Itercalation-enhanced electric polarization and chain formation of nano-layered particles* Europhysics Letters, 74, 3, 438-444, 2006
29. Friese, K., Krüger, H., Kahlenberg, V ., Balic-Zunic, T ., Emerich, H ., Gesland, J-Y., Grzechnik, A . *Study of the temperature dependence of the structure of KY_3F_{10}* J. Phys.: Condens. Matter 18, 2677-2687, 2006
30. Grzechnik, A., Balic-Zunic, T., Makovicky, E., Gesland, J.-Y., Friese, K. *The compressibility mechanism of $Li_3Na_3In_2F_{12}$ garnet* J. Phys.: Condens. Matter, 18, 2915-2924, 2006
31. Gualtieri, A.F., Aprea, P. *The structure of K-hydrosodalite* Microp.& Mesop. Mater., 96, 1-3, 276-286, 2006
32. Gualtieri, A. F., Ferrari, S., Galli, E., Di Renzo, F., Van Beek, W. *Rietveld structure refinement of Zeolite ECR-1* Chem. Mater., 18, 1, 76 -84, 2006
33. Helland, R., Larsen, A. N., Smalås, A. O., Willassen, N. P. *The 1.8 Å crystal structure of a proteinase K-like enzyme from a psychrotroph Serratia species* FEBS J., 273, 61-71, 2006
34. Hernandez, O., Knight, K.S., Van Beek, W., Boucekkine, A., Boudjada, A. , Paulus, W., Meinnel, J. *Phases II and IV of 1,3,5-trichloro-2,4,6-trimethylbenzene: Ab initio crystal structure determination by high-resolution powder diffraction* J. Molecular Structure, 791, 1-3 , 41-52, 2006
35. Hersleth, H.-P., Ryde,U., Rydberg, P., Görbitz, C.H., Andersson, K.K. *Structures of the high-valent metal-ion haem-oxygen intermediates in peroxidases, oxygenases and catalases* J. Inorg.Biochemistry, 100, 4, 460-476, 2006
36. Huber, F., Yu, Zh., Lögdberg, S., Rønning, M., Chen, D., Venvik, H., Holmen, A. *Remarks on the passivation of reduced Cu-, Ni-, Fe-, Co-based catalysts* Catalysis Letters, 110, 3-4, 2006
37. Kantor, A. P., Kantor, I. Yu., Dubrovinsky, L. S., Krisch, M., Bossak, A., Dmitriev, V. P., Urusov, V. S. *Measuring the speed of sound in an iron-nickel alloy at high pressure by inelastic X-ray scattering* Doklady Physics, 51,11, 584-587, 2006
38. Krivovichev, S.V., Chernyshov, D.Y., Döbelin, N., Armbruster, Th., Kahlenberg, V., Kaindl, R., Ferraris, G., Tessadri, R., Kaltenhauser, G. *Crystal chemistry and polytypism of tyrolite T*American Mineralogist, 91, 1378-1384, 2006
39. Kurnosov, A., Dubrovinsky, L., Kuznetsov, A., Dmitriev, V. *High-pressure / High-temperature behavior of the methane-ammonia-water system up to 3 GPa* Z. Naturforschung B, 61, 12, 1573-1579, 2006
40. Kuznetsov, A., Pereira, A., Shiryaev, A., Haines, J., Dubrovinsky, L., Dmitriev, V., Pattison, P., Guignot, N. *Pressure-Induced chemical decomposition and structural changes of Boric Acid* J. Phys. Chem. B, 110, 28, 13858 -13865, 2006
41. Leinekugel-le-Cocq, A.Y., Deniard, P., Jobic, S., Cerny, R., Bart, F., Emerich, H. *Synthesis and characterization of hollandite-type material intended for the specific containment of radioactive cesium* J. Solid State Chemistry, 179, 10, 3196-3208, 2006
42. Le Toquin, R., Paulus, W., Cousson, A., Prestipino, C., Lamberti, C. *Time-resolved in situ studies of oxygen intercalation into $SrCoO_{2.5}$, performed by neutron diffraction and X-ray absorption spectroscopy* J. Am. Chem. Soc., 128, 40, 13161-13174, 2006
43. Llewellyn, Ph.L., Bourrelly, S., Serre, Ch., Filinchuk, Y., Férey, G. *How hydration drastically improves adsorption selectivity for CO2 over CH4 in the Flexible Chromium Terephthalate MIL-53* Angew. Chem. Int., 45, 46, 7751 - 7754, 2006
44. Luechinger, M., Kienhöfer, A., Pirngruber, G. D. *Immobilized complexes of metals with Amino Acid Ligands - a first step toward the development of new biomimetic catalysts* Chem. Mater., 18, 5, 1330 -1336, 2006
45. Machon, D., McMillan, P. F., Xu, B., Dong, J. *High-pressure study of the β-to-α transition in Ga_2O_3* Phys. Rev. B, 73, 094125, 2006
46. Marichal, C., Chézeau, J. M., Roux, M., Patarin, J., Jordá, J. L., McCusker, L. B., Baerlocher, Ch., Pattison, Ph. *Synthesis and structure of Mu-33, a new layered*

aluminophosphate $|((CH_3)_3CNH_3^+)_{16}(H_2O)_4|[Al_{16}\ P_{24}O_{88}(OH)_8]$ Microp. & Mesop. Materials, 90, 1-3, 5-15, 2006

47. Méheust, Y., Knudsen, K.D., Fossum, J.O. *Inferring orientation distributions in anisotropic powders of nano-layered crystallites froma single two-dimensional WAXS image* J.Applied Cryst., 39, 5, 661-670, 2006
48. Mentzen, B. F., Bergeret, G., Emerich, H., Weber, H.-P. *Dehydrated and Cs^+-exchanged MFI Zeolites: location and population of Cs^+ from in situ diffraction data as a function of temperature and degree of exchange* J. Phys. Chem., 110, 1, 97 -106, 2006
49. Mentzen, B. F., Bergeret, G., Emerich, H., Weber, H.-P. *Hydrated Cs^+-exchanged MFI Zeolites: location and population of Cs^+ cations and water molecules in hydrated $Cs_{6.6}$MFI from in and ex situ powder X-ray diffraction data as a function of temperature and other experimental conditions* J. Phys. Chem. B, 110, 28, 13741 -13752, 2006
50. Mentzen, B. F., Tuel, A., Bayard, F. *Location of the tripropylbenzylammonium ion (P3BZY) in the as-synthesized zeolite ZSM-5 (Si/Al = 28): A study by solid-state NMR, computer simulations and X-ray synchrotron powder diffraction* Microp.& Mesop. Mat., 93, 171-179, 2006
51. Moe, E., Leiros, I., Smalås, A.O., McSweeney, S. *The crystal structure of mismatch-specific Uracil-DNA glycosylase (MUG) from Deinococcus radiodurans reveals a novel catalytic residue and broad substrate specificity* J. Biol. Chem., 281, 1, 569-577, 2006
52. Nakamura, Y., Fossdal, A., Brinks, H.W., Hauback, B.C. *Characterization of Al–Ti phases in cycled TiF_3-enhanced Na_2LiAlH_6* J. Alloys and Compounds, 416, 1-2, 274-278, 2006
53. Nazaralya, M., Wallez, G., Chanéac, C., Tronc, E., Ribot, F., Quarton, M., Jolivet, J. -P. *Synthesis and characterization of $Ce^{IV}(PO_4)(HPO_4)_{0.5}(H_2O)_{0.5}$* J. Physics & Chemistry of Solids, 67, 5-6, 1075-1078, 2006
54. Petukhov, A. V., Thijssen, J. H. J., 't Hart, D. C., Imhof, A., Van Blaaderen, A., Dolbnya, I. P., Snigirev, A., Moussaïd, A., Snigireva, I. *Microradian X-ray diffraction in colloidal photonic crystals* J. Appl. Cryst. 39, 137-144, 2006
55. Plazanet, M., Dean, M., Merlini, M., Huller, A., Emerich, H., Meneghini,C., Johnson, M.R., Trommsdorff, H.P. *Crystallization on heating and complex phase behavior of α-cyclodextrin solutions* J. Chem. Phys. 125, 154504-154510, 2006
56. Poulsen, R.D., Bentien, A., Christensen, M., Iversen, B.B. *Solvothermal synthesis, multi-temperature crystal structures and physical properties of isostructural coordination polymers, $2C_4H_{12}N^+$-$[M_3(C_8H_4O_4)_4]^{2-}\cdot 3C_5H_{11}NO$, M = Co, Zn* Acta Cryst., B62, 245-254, 2006
57. P. Ravindran, R. Vidya, A. Kjekshus, and H. Fjellvåg, O. Eriksson *Theoretical investigation of magnetoelectric behavior in* $BiFeO_3$ Phys. Rev. B, 74, 224412-224430, 2006
58. Reehuis, M., Ulrich, C., Pattison, P., Ouladdiaf, B., Rheinstädter, M. C., Ohl, M., Regnault, L. P. & al. *Neutron diffraction study of YVO_3, $NdVO_3$, and $TbVO_3$* Phys. Rev. B, 73, 094440, 2006
59. Reehuis, M., Ulrich, C., Proke, K., Gozar, A., Blumberg, G., Komiya, S., Ando, Y., Pattison, P., Keimer, B. *Crystal structure and high-field magnetism of La_2CuO_4* Phys. Rev. B, 73, 144513, 2006
60. Riise, E. K., Lorentzen, M. S., Helland, R., Willassen, N. P. *Crystallization and preliminary X-ray diffraction analysis of a cold-adapted catalase from Vibrio salmonicida* Acta Cryst. F, 62, 77-79, 2006
61. Scheidegger, A.M., Vespa, M., Grolimund, D., Wieland, E., Harfouche, M., Bonhoure, I., Dähn, R. *The use of (micro)-X-ray absorption spectroscopy in cement research* Waste Management, 26, 7, 699-705 , 2006
62. Serre, Ch., Millange, F., Devic, Th., Audebrand, N., Van Beek, W. *Synthesis and structure determination of new open-framework chromium carboxylate MIL-105 or $Cr^{III}(OH)^*\{O_2C\text{-}C_6(CH_3)_4\text{-}CO_2\}^*nH_2O$* Material Res. Bulletin, 41, 8, 1550-1557, 2006
63. Shustova, N., Chernyshev, D., Troyanov, S. *Crystal structure of $C_{60}Cl_6$ prepared by a reaction of C_{60} with $POCl_3$* Mendeleev Comm., 209-210, 2006
64. Søgaard, M., Hendriksen, P.V., Mogensen, M., Poulsen, F.W., Skou, E.

Oxygen nonstoichiometry and transport properties of strontium substituted lanthanum cobaltite Solid State Ionics, 177, 37-38, 3285-3296, 2006

65. Sørby, M.H., Brinks, H.W., Fossdal, A., Thorshaug, K., Hauback, B.C. *The crystal structure and stability of K_2NaAlH_6* J. Alloys and Compounds, 415, 1-2, 284-287, 2006
66. Swamy, V., Menzies, D., Muddle, B.C., Kuznetsov, A., Dubrovinsky, L., Dai, Q., Dmitriev, V. *Nonlinear size dependence of anatase TiO_2 lattice parameters* Appl. Phys. Lett. 88, 243103, 2006
67. Thorkildsen, G., Larsen, H. B., Beukes, J. A. *Angle calculations for a three-circle goniostat* J. Appl. Cryst., 39, 151-157, 2006
68. Tkalcec, I., Mari, D., Benoit, W. *Correlation between internal friction background and the concentration of carbon in solid solution in a martensitic steel* Mater. Science & Engineering: A, 442, 1-2, 471-475, 2006
69. Tokaychuka, Ya.O., Bodak, O.I., Gorelenko, Yu, K., Yvon, K. *Structural and magnetic properties of iron-rich compounds in the Yb–Fe–Ga system* J. Alloys and Compounds, 415, 1-2, 8-10, 2006
70. Törnroos, K.W., Hostettler, M., Chernyshov, D., Vangdal, B., Bürgi, H.-B. *Interplay of spin conversion and structural phase transformations: reentrant phase transitions in the 2-Propanol Solvate of Tris(2-picolylamine)iron(II) Dichloride* Chem. Eur.J., 12, 24, 6207 - 6215 , 2006
71. Van Mechelen, J. B., Peschar, R., Schenk, H. *Structures of mono-unsaturated triacylglycerols. I. The β2 polymorph* Acta Cryst., B62, 1121-1130, 2006
72. Van Mechelen, J. B., Peschar, R., Schenk, H. *Structures of mono-unsaturated triacylglycerols. II. The β2 polymorph* Acta Cryst., B62, 1131-1138, 2006
73. Vespa, M., Dähn, R., Gallucci, E., Grolimund, E., Wieland, E., Scheidegger, A.M. *Microscale investigations of Ni uptake by cement using a combination of scanning electron microscopy and synchrotron-based techniques* Environ. Sci. Technol., 40, 7702-7709, 2006
74. Vespa, M., Dähn, R., Grolimund, D., Harfouche, M., Wieland, E., Scheidegger, A. M. E. *Speciation of heavy metals in cement-stabilized waste forms: a micro-spectroscopic study* J. Geochem. Exploration, 88, 1-3, 77-80, 2006
75. Vespa, M., Dähn, R., Grolimund, D., Wieland, E., Scheidegger, A. M. *Spectroscopic investigation of Ni speciation in hardened cement paste* Environ. Sci. Technol., 40, 7, 2275 -2282, 2006
76. Vespa, M., Dähn, R., Wieland, E., Grolimund, D., Scheidegger, A. M. *The influence of hydration time on the Ni uptake by cement* Czechoslovak J. Physics, 56, suppl. D, 2006
77. Vrålstad, T., Glomm, W.R., Ronning, M., Dathe, H., Jentys, A., Lercher, J.A., Øye, G., Stöcker, M., Sjöblom, J. *Spectroscopic characterization of cobalt-containing mesoporous materials* J. Phys. Chem. B, 110, 11, 5386 -5394, 2006
78. Wallez, G., Clavier, N., Dacheux, N., Quarton, M., Van Beek, W. *From thorium phosphate hydrogenphosphate hydrate to ß-thorium phosphate diphosphate: Structural evolution to a radwaste storage ceramic* J. Solid State Chemistry, 179,10, 3007-3016, 2006
79. Weber, Th., Kobas, M., Steurer, W. *Phasonic disorder in decagonal Al–Co–Ni* Philosophical Magazine, 86, 3-5, 537 - 542, 2006
80. Weiher, N., Bus, E., Delannoy, L., Louis, C., Ramaker, D.E., Miller, J.T., Van Bokhoven, J.A. *Structure and oxidation state of gold on different supports under various CO oxidation conditions* J. Catalysis, 240, 2, 100-107, 2006
81. Zanardi, S., Carati, A., Cruciani, G., Bellussi, G., Millini, R., Rizzo, C. *Synthesis, characterization and crystal structure of new microporous bismuth silicates* Microp.& Mesop. Mater., 97, 1-3, 34-41, 2006
82. Zbinden, K. G., Banner, D. W., Hilpert, K., Himber, J., Lavé, Th., Riederer, M. et al. *Dose-dependent antithrombotic activity of an orally active tissue factor/factor VIIa inhibitor without concomitant enhancement of bleeding propensity* Bioorganic & Medicinal Chemistry, 14,15, 5357-5369, 2006